

# The Evolution of Globular Clusters in the Galaxy

Koji Takahashi <sup>1</sup>

Department of Earth Science and Astronomy,  
College of Arts and Sciences, The University of Tokyo,  
3-8-1 Komaba, Meguro-ku, Tokyo 153-8902, Japan  
takahasi@chianti.c.u-tokyo.ac.jp

and

Simon F. Portegies Zwart <sup>2</sup>

Department of Astronomy, Boston University,  
725 Commonwealth Avenue, Boston, MA 01581  
spz@komodo.bu.edu

## ABSTRACT

We investigate the evolution of globular clusters using  $N$ -body calculations and anisotropic Fokker-Planck calculations. The models include a mass spectrum, mass loss due to stellar evolution, and the tidal field of the parent galaxy. Recent  $N$ -body calculations have revealed a serious discrepancy between the results of  $N$ -body calculations and isotropic Fokker-Planck calculations. The main reason for the discrepancy is an oversimplified treatment of the tidal field employed in the *isotropic* Fokker-Planck models. In this paper we perform a series of calculations with *anisotropic* Fokker-Planck models with a better treatment of the tidal boundary and compare these with  $N$ -body calculations. The new tidal boundary condition in our Fokker-Planck model includes one free parameter. We find that a single value of this parameter gives satisfactory agreement between the  $N$ -body and Fokker-Planck models over a wide range of initial conditions.

Using the improved Fokker-Planck model, we carry out an extensive survey of the evolution of globular clusters over a wide range of initial conditions varying the slope of the mass function, the central concentration, and the relaxation time. The evolution of clusters is followed up to the moment of core collapse or the disruption of the clusters in the tidal field of the parent galaxy. In general, our model clusters, calculated with the anisotropic Fokker-Planck model with the improved treatment for the tidal boundary, live longer than isotropic models. The difference in the lifetime between the isotropic and anisotropic models is particularly large when the effect of mass loss via stellar evolution is rather significant. On the other hand the difference is small for relaxation-dominated clusters which initially have steep mass functions and high central concentrations.

*Subject headings:* Galaxy: kinematics and dynamics — galaxies: kinematics and dynamics — galaxies: star clusters — globular clusters: general — open clusters and associations: general — methods: numerical

---

<sup>1</sup>Present address: Department of Astronomy, School of Science, The University of Tokyo, 7-3-1 Hongo, Bunkyo-ku, Tokyo 113-0033, Japan

<sup>2</sup>Hubble Fellow

## 1. Introduction

The most reliable method to model the evolution of dense star clusters is the direct integration of the equations of motions of all stars via  $N$ -body calculations. The high cost of such calculations, however, limits the choice of the number of stars to a few ten thousands, a small number compared to real globular clusters, and also limits the number of calculations which can be performed on a practical time scale.

In the last few decades Fokker-Planck models have gained in popularity for studying the dynamics of globular clusters (see Meylan & Heggie 1997 for a recent review). The relatively low computational cost of Fokker-Planck models makes it possible to perform a large number of calculations over broad ranges of initial parameters. This opens the possibility to study the initial parameter space which may have been available at the formation of the population of observed globular clusters.

On the other hand, one has to pay for the higher speed of Fokker-Planck calculations with a less accuracy of these models. It is therefore important to examine the accuracy of Fokker-Planck models. One way of such examinations is to do a comparative study between Fokker-Planck and  $N$ -body calculations.

### 1.1. What happened before

The development of approximate methods for modeling the dynamical evolution of star clusters started in the 1970's using Monte-Carlo methods (Spitzer 1987, and references therein). Several groups applied these methods to address various problems in stellar dynamics. Cohn (1979, 1980) developed a new method in which the orbit-averaged Fokker-Planck equation was solved directly using a finite-difference technique. Cohn (1980) demonstrated that his code could follow the evolution of the cluster into much more advanced stages of core collapse than Monte-Carlo codes (see, however, Giersz 1998, for a possible revival of Monte-Carlo methods).

In Cohn's calculations globular clusters were modeled as fairly idealized systems, i.e.: isolated systems of identical point masses (Cohn 1979, 1980). This is quite a natural starting point for theoretical studies. After Cohn's seminal works, many contributions have been made to improve Cohn's Fokker-Planck scheme in terms of adding various astrophysical processes, such as a mass spectrum, primordial binaries, a tidal cut-off, gravitational shocks by the galactic disk and bulge, mass loss from stellar evolution, anisotropy of the velocity distribution, rotation of the clusters, etc. (see Meylan & Heggie 1997).

An important landmark in modeling the evolution of globular clusters with Fokker-Planck calculations was set by Chernoff & Weinberg (1990, hereafter CW). Their models included a tidal cut-off by the parent galaxy, a stellar mass spectrum, and mass loss due to stellar evolution.

CW boldly added simultaneously several new astrophysical phenomena to their models. However, generally speaking, each time a model is extended trying to make simulations more "realistic", the number of assumptions usually increases; therefore thorough testing is required (not only for Fokker-Planck models) to eliminate the possible introduction of omissions and the violation of previously-made assumptions. It is not easy to assess the reliability of a model. The most reliable way to do this may well be detailed comparison with another model which is based on a completely different numerical method.

Such comparisons have found good agreement between  $N$ -body, Fokker-Planck, and gaseous models for isolated star clusters of point masses (Giersz and Heggie 1994a, 1994b; Giersz and Spurzem 1994; Spurzem and Takahashi 1995). These are important results because they demonstrate that two-body relaxation is a

main physical process which drives the dynamical evolution of star clusters, as was expected from theory (see, e.g., Spitzer 1987), and therefore that the time evolution of such relatively simple systems scales with the two-body relaxation time.

Fukushige & Heggie (1995) and Portegies Zwart et al. (1998) demonstrated that  $N$ -body calculations give significantly different results from the isotropic Fokker-Planck calculations of CW for some initial conditions. These  $N$ -body and Fokker-Planck calculations included the steady tidal field of the parent galaxy and mass loss due to the evolution of single stars. The results of Portegies Zwart et al. (1998) can be summarized as follows: 1) The clusters simulated with the  $N$ -body model live more than an order of magnitude longer than the comparable isotropic Fokker-Planck model; 2) The lifetime of the clusters depends on the number of stars  $N$  in a rather complex way. The clusters with a larger number of stars live shorter contrary to what was expected). A similar  $N$ -dependence of  $N$ -body models was also found in a collaborative experiment organized by Heggie (Heggie et al. 1999).

Takahashi & Portegies Zwart (1998, TPZ hereafter) solved the discrepancies pointed out by Portegies Zwart et al. (1998) by using more general *anisotropic* Fokker-Planck models together with an improved treatment of the tidal boundary. The improved Fokker-Planck models are in excellent agreement with  $N$ -body models.

The assumption of velocity isotropy and the oversimplified escape condition adopted by CW turned out to result in an enormous overestimate of the escape rate, i.e.: an underestimate of the life time of the cluster. TPZ took account of the orbital angular momentum as well as the orbital energy to determine escaping stars. TPZ also took account of that a star on an escape orbit requires some time to leave the cluster. The number of stars that escape per relaxation time depends therefore on the ratio of the relaxation time to the dynamical time, i.e.: on the number of stars.

TPZ’s implementation of the escape condition adds a free parameter  $\nu_{\text{esc}}$  (denoted by  $\alpha_{\text{esc}}$  in TPZ) to Fokker-Planck models. This parameter determines the time scale on which escaping stars leave the cluster, and should be of the order of the crossing time at the tidal radius (Lee & Ostriker 1987; see also Ross et al. 1997). TPZ compared Fokker-Planck calculations with  $N$ -body calculations to calibrated  $\nu_{\text{esc}}$  for one specific set of initial conditions: density profile, mass function and relaxation time. However, it is not obvious that a single value of  $\nu_{\text{esc}}$  gives good agreement between Fokker-Planck and  $N$ -body models for a wide range of initial conditions. To test this hypothesis is the first main purpose of this paper.

The second purpose of this paper is to carry out an extensive survey of the evolution of globular clusters in the Galaxy for various initial conditions. The same initial conditions will be used as those of the survey by CW. We perform the survey with the improved anisotropic Fokker-Planck models with the calibrated value for  $\nu_{\text{esc}}$ .

In the following section we review the anisotropic Fokker-Planck model and the  $N$ -body model. In section 3 the stellar evolution models are described, and the initial conditions are reviewed in section 4. The results of a comparison between Fokker-Planck and  $N$ -body models are presented in section 5. Fokker-Planck survey results are shown in section 6. Section 7 discusses our simulation results, including comparison with other  $N$ -body simulations and with observations. We summarize our findings in section 8.

## 2. The Models

## 2.1. The Fokker-Planck model

We use anisotropic orbit-averaged Fokker-Planck models (Cohn 1979; Takahashi 1995). The star cluster is assumed to be spherically symmetric and in dynamical equilibrium at any time. The distribution function  $f$  at time  $t$  is then a function of the energy of a star per unit mass,  $E$ , and the angular momentum per unit mass,  $J$  (see e.g., Spitzer 1987, section 1.2). On the other hand, isotropic Fokker-Planck models (Cohn 1980) assume that the distribution function does not depend on the angular momentum, i.e., that the velocity distribution is isotropic at every point in the cluster.

Anisotropic Fokker-Planck models are more general than isotropic Fokker-Planck models and therefore preferable. The higher computational costs and more complex numerical implementation, however, caused anisotropic Fokker-Planck models to be less favored than their isotropic cousins (Cohn 1980). The numerical problem which was encountered by Cohn (1979) in his anisotropic Fokker-Planck calculations was solved by Takahashi (1995; 1996) mainly by implementing a new finite-difference scheme (see also Drukier et al. 1999).

All Fokker-Planck calculations in this paper are performed with the code which was developed by Takahashi (1995; 1996) and was later modified to include a mass function for single stars (Takahashi 1997), a tidal boundary (Takahashi et al. 1997; TPZ), and stellar evolution (TPZ).

### 2.1.1. Determination of escaping stars

TPZ demonstrated that the results of Fokker-Planck calculations are sensitive to the choice of the tidal boundary conditions. Two different criteria for the identification of escapers were tested by Takahashi et al. (1997) and by TPZ. These are: 1) the apocenter criterion, in which a star is removed if

$$r_a(E, J) > r_t; \quad (1)$$

and 2) the energy criterion, in which a star is removed if

$$E > E_t \equiv -GM/r_t. \quad (2)$$

Here  $r_t$  is the tidal radius of the cluster,  $r_a(E, J)$  is the apocenter distance of a star with energy  $E$  and angular momentum  $J$ ,  $G$  is the gravitational constant, and  $M$  is the cluster mass.

The apocenter criterion is considered more realistic than the energy criterion. The latter tends to remove too many stars too quickly, since it may even remove stars orbiting inside the tidal radius. For most calculations we adopt the apocenter criterion to determine escapers for Anisotropic Fokker-Planck models; we call these models Aa models. We also adopt the energy criterion for some calculations, these models are called Ae models.

### 2.1.2. Introducing the crossing time in the Fokker-Planck model

In the Fokker-Planck calculations performed by CW, escapers are removed instantaneously from the clusters. In the absence of stellar evolution this condition may be justified if the dynamical time scale of the cluster is negligible compared to the two-body relaxation time, i.e.; if the number of stars  $N \rightarrow \infty$ .

TPZ demonstrated that the lifetime of stellar systems with small  $N$  is dramatically affected by the time scale on which escaping stars are removed from the cluster. Two treatments of escaping stars were tested by TPZ: 1) instantaneous escape: a star is removed from the cluster as soon as it satisfies an adopted escape criterion; 2) crossing-time escape: a star on an escape orbit hangs around in the cluster for a certain time before it really leaves the cluster.

To implement the crossing-time escape condition in Fokker-Planck calculations we use the boundary condition of Lee & Ostriker (1987):

$$\frac{\partial f}{\partial t} = -\nu_{\text{esc}} f \left[ 1 - \left| \frac{E}{E_t} \right|^3 \right]^{1/2} \frac{1}{2\pi} \sqrt{\frac{4\pi}{3}} G \rho_t. \quad (3)$$

Here  $\rho_t$  is the mean mass density within the tidal radius and  $\nu_{\text{esc}}$  is a dimensionless constant which determines the time scale on which escapers leave the cluster. This equation is applied in a region of phase space where the adopted escape criterion is satisfied. Eq. (3) is derived assuming that escapers leave the cluster on a dynamical time scale. For  $N \rightarrow \infty$  with a fixed relaxation time, this condition becomes identical to removing escapers instantaneously, since the ratio of the crossing time to the relaxation time vanishes.

When Eq. (3) is used, the density at the tidal radius is generally still finite. The total mass of the cluster is then defined by the mass within  $r_t$ .

### 2.1.3. The mass function

In our Fokker-Planck models a continuous mass function is represented by  $K$  discrete mass components. We use  $K = 20$  components for all Fokker-Planck calculations. This number is considered to be sufficiently large for our calculations (see CW). At  $t = 0$  the mass of a star in mass-bin  $k$  is given by

$$m_k = m_- \left( \frac{m_+}{m_-} \right)^{(k-\frac{1}{2})/K}. \quad (4)$$

Here  $m_-$  and  $m_+$  are the lower and upper limits of the initial mass function. The total mass in mass interval  $k$  is

$$M_k = \int_{m_{k-\frac{1}{2}}}^{m_{k+\frac{1}{2}}} \frac{dN}{dm} m dm. \quad (5)$$

Here  $dN/dm$  is the number of stars per unit mass interval.

## 2.2. The $N$ -body model

The  $N$ -body portion of the simulations is carried out using the **Kira** integrator, operating within the Starlab (version 3.3) software environment (McMillan & Hut 1996; Portegies Zwart et al. 1998). Time integration of stellar orbits is accomplished using a fourth-order Hermite scheme (Makino & Aarseth 1992). **Kira** also incorporates block time steps (McMillan 1986a; 1986b; Makino 1991), special treatment of close two-body and multiple encounters of arbitrary complexity, and a robust treatment of stellar and binary evolution and stellar collisions (Portegies Zwart et al. 1999). The special-purpose GRAPE-4 (Makino et al. 1997) system is used to accelerate the computation of gravitational forces between stars. The treatment of stellar mass loss is described in Portegies Zwart et al. (1998). A more complete description

of the Starlab environment is in preparation, but more information can be found at the following URL: <http://www.ias.edu/~starlab>.

### 3. Stellar Evolution

#### 3.1. $N$ -body Models

Stars in the  $N$ -body calculations are evolved with the stellar evolution model **SeBa**<sup>3</sup> (Portegies Zwart & Verbunt 1996, Section 2.1). In **SeBa** stars with mass  $m > 8M_\odot$  become neutron stars with mass  $m_{\text{fin}} = 1.34M_\odot$ , and lower mass stars become white dwarfs. The mass of these white dwarfs are given by the core mass of their progenitors.

The evolution of the stars in the Fokker-Planck calculations which are compared with the  $N$ -body runs is also computed using **SeBa**. In practice tabulated data as listed in Table 1 are used.

#### 3.2. Fokker-Planck models

We use the same stellar evolution model as was adopted by CW when we compare our anisotropic Fokker-Planck models with CW’s models. The stars in this stellar evolution model live somewhat shorter than those in **SeBa** (see Table 1).

Table 1 compares the stellar evolution model used by CW with **SeBa**. The main-sequence lifetimes in the CW model are obtained by fitting cubic splines to the data listed in Table 1 of CW. They do not mention the lifetimes of stars with mass  $m \leq 0.83M_\odot$ . Some clusters become considerably older than 15 Gyr and it is necessary to use proper lifetimes for these stars as well. We assume that the lifetime of stars with  $m \leq 0.83M_\odot$  is proportional to  $m^{-3.5}$  (Drukier 1995). This extrapolation gives also a good fit to the lifetime of the low-mass stars in **SeBa** (see Table 1).

At the end of the main-sequence life, a star with an initial mass  $m_{\text{ini}}$  forms a compact object with mass  $m_{\text{fin}}$ . In the model adopted by CW the remnant mass is given by

$$m_{\text{fin}} = \begin{cases} 0.58 + 0.22(m_{\text{ini}} - 1), & \text{for } m_{\text{ini}} < 4.7 [M_\odot], \\ 0, & \text{for } 4.7 \leq m_{\text{ini}} \leq 8.0 [M_\odot], \\ 1.4, & \text{for } 8.0 < m_{\text{ini}} \leq 15.0 [M_\odot]. \end{cases} \quad (6)$$

Stars with mass  $m_{\text{ini}} \lesssim 0.46 M_\odot$  do not lose any mass in a stellar wind as they turn into white dwarfs.

The implementation in the Fokker-Planck model is as follows: The mass of the  $k$ -th component (see § 2.1.3) is decreased from its initial mass  $m_k^{\text{ini}}$  to the final (remnant) mass  $m_k^{\text{fin}}$  linearly with time  $t$  during the interval  $t_{\text{MS}}(m_{k+1/2}^{\text{ini}}) < t < t_{\text{MS}}(m_{k-1/2}^{\text{ini}})$ , where  $t_{\text{MS}}(m)$  is the main-sequence lifetime of a star with mass  $m$ .

---

<sup>3</sup>The name **SeBa** is adopted from the Egyptian word for ‘to teach’, ‘the door to knowledge’ or ‘(multiple) star’. The exact meaning depends on the hieroglyphic spelling.

#### 4. Initial Conditions

The initial conditions for our Fokker-Planck and  $N$ -body calculations are identical to those of the survey performed by CW. It is assumed that the galaxy has a flat rotation curve and the star clusters are on circular orbits with  $v_g = 220$  km/s around the galactic center. The tidal radius changes with time as  $r_t(t) \propto M^{1/3}(t)$ . The initial density profiles of the star clusters are set up from King models (King 1966). Calculations are performed with three different values of  $W_o = 1, 3$  and  $7$ , where  $W_o$  is the dimensionless central potential of the King models. The initial mass function is given by

$$dN \propto m^{-\alpha} dm, \quad (7)$$

with  $\alpha = 1.5, 2.5$  and  $3.5$  between  $m = 0.4 M_\odot$  and  $15 M_\odot$ .

In addition to the two dimensionless parameters  $W_o$  and  $\alpha$ , there is one more free parameter: the initial relaxation time. Following CW, the mean relaxation time within the tidal radius is defined as

$$t_{\text{rlx,CW}} = \frac{M^{1/2} r_t^{3/2}}{G^{1/2} m_\star \ln N}, \quad (8)$$

(eq. [6] of CW with  $r = r_t$  and  $c_1 = 1$ ), where  $m_\star$  is a representative stellar mass. This equation can be rewritten with setting  $m_\star = M_\odot$  as

$$t_{\text{rlx,CW}} = 2.57 \times 10^6 \text{ yr } F_{\text{CW}}, \quad (9)$$

where

$$F_{\text{CW}} \equiv \frac{M}{[M_\odot]} \frac{R_g}{[\text{kpc}]} \frac{[220 \text{ km s}^{-1}]}{v_g} \frac{1}{\ln N} \quad (10)$$

defines the cluster family (see CW). Here  $R_g$  is the distance to the Galactic center and  $v_g$  is the circular speed of the cluster around the Galactic center (cf. eqs. [1] and [2] of CW). The crossing time of the cluster is then

$$t_{\text{cr}} \approx \left( \frac{r_t^3}{GM} \right)^{1/2} = t_{\text{rlx,CW}} \frac{[M_\odot]}{M} \ln N. \quad (11)$$

A group of clusters of the same family (the same  $F_{\text{CW}}$ ) have the same initial relaxation time (9). Our survey covers CW's families 1, 2, 3 and 4. Table 2 reviews the properties of the selected families. For convenience Table 2 also gives the more usual half-mass relaxation time (Spitzer 1987, p. 40),

$$\begin{aligned} t_{\text{rh}} &= 0.138 \frac{M^{1/2} r_h^{3/2}}{G^{1/2} \langle m \rangle \ln N} \\ &= 3.54 \times 10^5 \text{ yr } F_{\text{CW}} \left( \frac{r_h}{r_t} \right)^{3/2} \frac{[M_\odot]}{\langle m \rangle}, \end{aligned} \quad (12)$$

where  $r_h$  is the half-mass radius and  $\langle m \rangle$  is the mean stellar mass.

#### 5. Comparison between Fokker-Planck and $N$ -body Models

We compare the results of anisotropic Fokker-Planck calculations (Aa models) and those of  $N$ -body calculations. The escaping stars in the Fokker-Planck models are removed on a crossing time scale using Eq. (3), but first we have to calibrate the value for  $\nu_{\text{esc}}$ .

### 5.1. The calibration of $\nu_{\text{esc}}$

The rate of mass loss in the Fokker-Planck models changes monotonically with  $\nu_{\text{esc}}$ ; larger  $\nu_{\text{esc}}$  causes the models to lose mass on a shorter time scale. Increasing  $\nu_{\text{esc}}$  has qualitatively the same effect on the mass loss speed as increasing  $N$  (i.e. increasing  $t_{\text{rlx}}/t_{\text{cr}}$ ) with  $\nu_{\text{esc}}$  held fixed.

The right choice of the initial conditions with which  $\nu_{\text{esc}}$  should be calibrated is rather subtle (TPZ). We use a wide range of initial conditions to find the most appropriate value for  $\nu_{\text{esc}}$ . No statistical analysis is performed for deciding which value of  $\nu_{\text{esc}}$  is the best, since the criterion with which a statistical test should comply is not clear. Rather we judge from global agreement in mass evolution by eye.

Figure 1 shows the total mass evolution for Fokker-Planck calculations with  $\nu_{\text{esc}} = 2, 2.5$ , and 3 for selected initial models and compares them with  $N$ -body calculations. These initial models were selected because stellar evolution as well as two-body relaxation play a significant role for these models.

For the models shown in the top two panels,  $\nu_{\text{esc}} = 3$  gives good agreement between the Fokker-Planck and  $N$ -body models at later epochs for  $N = 1\text{K}$ ; For  $N = 16\text{K}$  and  $32\text{K}$ , a value of  $\nu_{\text{esc}}$  between 2 and 2.5 is preferable, except for the final phase. For the models shown in the middle panels,  $\nu_{\text{esc}} = 3$  gives good agreement for the entire evolution. For the models shown in the bottom panels, the evolution is rather insensitive to  $\nu_{\text{esc}}$  as well as  $N$ , and the agreement between the Fokker-Planck and  $N$ -body models is good.

From these comparisons we conclude that the best agreement between  $N$ -body and Fokker-Planck models is achieved for  $2 < \nu_{\text{esc}} < 3$ , and we adopt the median value of  $\nu_{\text{esc}} = 2.5$  for the rest of our calculations.

### 5.2. The time evolution of the total mass

Here we present comparisons between  $N$ -body and Fokker-Planck calculations for various initial conditions. A part of the results were already presented in the previous subsection, but are reproduced here with new information.

TPZ performed Fokker-Planck calculations for the initial model of  $W_0 = 3$ ,  $\alpha = 2.5$  and family 1 with using  $\nu_{\text{esc}} = 2$ . Fig. 2a shows repeated calculations with the new adopted value of  $\nu_{\text{esc}} = 2.5$ . We also perform  $N$ -body and Fokker-Planck calculations with initially 8K and 16K stars for other selected sets of initial conditions (for economical reasons one set of initial conditions is computed with only 4K and 8K stars); see Figs. 2b–f. The  $N$ -body calculations are continued up to 10 Gyr unless disruption occurs before this time. To see the convergence for  $N \rightarrow \infty$  one extra Fokker-Planck calculation for each set of initial conditions is performed with the instantaneous escape condition.

The dash-dotted lines in Fig. 2 represent the expected evolution of the total mass when no escapers are allowed, i.e., when mass loss occurs only through stellar evolution. They give upper limits to the cluster mass at each instance. (The  $N$ -body model of Fig. 2a with 1K stars seems to lose mass less quickly than the pure stellar-evolution mass loss case! But this is caused by random rendering in the small number of stars.)

Fig. 3 shows the time evolution of the relative difference in the total mass between the Fokker-Planck and  $N$ -body models, which we define as  $[M_{\text{F-P}}(t) - M_{N\text{-body}}(t)]/M_{N\text{-body}}(t)$ . The rapid increase of the relative difference seen in the upper two panels of Fig. 3 is the result of the disruption of the  $N$ -body models.



Fig. 4 plots the dimensionless mass loss rate  $\xi$  as a function of time, where time is expressed in units of the initial half-mass relaxation time  $t_{\text{rh0}}$ . The cluster mass loss rate  $dM/dt$  may be divided into two parts;

$$\frac{dM}{dt} = \left( \frac{dM}{dt} \right)_{\text{esc}} + \left( \frac{dM}{dt} \right)_{\text{se}}, \quad (13)$$

where the first term in the right-hand side represents the mass loss due to escapers from the tidal radius and the second term represents the mass loss due to stellar evolution. Since the stellar evolution is the same in the Fokker-Planck and  $N$ -body models, it may be useful to separate the stellar evolution mass loss from the total mass loss in order to further clarify the difference between the two models. Thus in Fig. 4 we plot the mass loss rate due to escapers  $\xi_{\text{esc}}$  as well as the total mass loss rate  $\xi_{\text{tot}}$  defined as follows:

$$\xi_{\text{tot}} = -\frac{t_{\text{rh0}}}{M} \frac{dM}{dt}, \quad \xi_{\text{esc}} = -\frac{t_{\text{rh0}}}{M} \left( \frac{dM}{dt} \right)_{\text{esc}}. \quad (14)$$

When there is no stellar evolution,  $\xi_{\text{esc}}$  is usually much less than 1 (Lee & Goodman 1995). This is to be expected, since in that case mass loss proceeds only on two-body relaxation time scale. In the present models, since the stellar evolution mass loss causes the shrink of the tidal radius and thus produces more escapers,  $\xi_{\text{esc}}$  exceeds 1 sometimes.

Fig. 2 as well as Figs. 3 and 4 show that the Fokker-Planck and  $N$ -body calculations agree fairly well over the entire range of initial conditions we investigated. Apparently the single value of  $\nu_{\text{esc}} = 2.5$  is applicable. The relative difference of the total mass at each time is generally less than 10%. However, for the cases of  $(W_o, \alpha, \text{family}) = (3, 2.5, 4)$  and  $(7, 1.5, 4)$ , the difference is rather large. This large difference seems to well correlate with large  $\xi_{\text{esc}} (> 1)$ , especially in the  $N$ -body models. Also when the cluster is about to dissolve (see panels [a] and [b]),  $\xi_{\text{esc}}$  becomes larger than 1 and the Fokker-Planck and  $N$ -body models deviate.

In the case of  $(W_o, \alpha, \text{family}) = (3, 2.5, 4)$ , the  $N$ -body models tend to lose mass more quickly than the Fokker-Planck models. The mass loss in the  $N$ -body models accelerates rapidly, compared with the Fokker-Planck models, from about 1 Gyr for the 16K model and from about 2 Gyr for the 8K model, and after some time the rate of mass loss decreases again. A similar behavior, with smaller amplitudes, is also observed for the other initial conditions. This phased mass loss is caused by a retardation effect in the  $N$ -body models. Each time the clusters lose mass by stellar evolution and by losing stars from the tidal boundary it requires several crossing times to fill up the outer layers of the cluster and to recover dynamical equilibrium. In this period mass loss mainly comes from stellar evolution only, which results in a temporary decrease in the rate of mass loss. Since the crossing time is long ( $t_{\text{cr}} \sim 1$  Gyr) in the models shown in Fig. 2d, such a phased mass loss is clearly seen in this case. (In the Fokker-Planck models dynamical equilibrium is assumed.) The large values of  $\xi_{\text{esc}}$  result from the rapid stellar-evolution-driven mass loss and the long relaxation time of these models ( $\xi_{\text{esc}}$  measures the fraction of mass lost per relaxation time).

The models with  $(W_o, \alpha, \text{family}) = (7, 1.5, 4)$  are characterized by a flat initial mass function and a high initial concentration. Fig. 2e shows that the cluster loses about 80% of its initial mass within the first billion years, and still remains bound. The mass loss is mainly driven by stellar evolution. The rather flat initial mass function causes about 33% (in number) of the stars to leave the main-sequence within 1 Gyr. The fraction of mass lost from the cluster due to stellar evolution alone is therefore about 62%. Nevertheless the cluster still survives beyond 10 Gyr. The cluster is saved by its initial high central concentration ( $W_o = 7$ ). In the first 1 Gyr the halo of the cluster is stripped almost completely, but the compact core survives. Even in this extreme case the agreement between Fokker-Planck and  $N$ -body models is fair. The difference between the Fokker-Planck and  $N$ -body models generally builds up in the first billion years (when  $\xi_{\text{esc}} > 1$ ),

and stays almost constant afterwards. The Fokker-Planck models assume that the potential change is adiabatic, but this assumption is clearly violated during the early rapid mass-loss period, since  $t_{\text{cr}} \sim 1$  Gyr.

The main results of this subsection are summarized as follows: 1) Aa Fokker-Planck models with  $\nu_{\text{esc}} = 2.5$  agree fairly well with  $N$ -body models in all the cases we investigated; 2) however, the agreement becomes worse when a large fraction of the total mass is lost on a crossing time scale. Such rapid mass loss conflicts with the assumption of the adiabatic potential change which the Fokker-Planck model is based on. In real globular clusters the number of stars is at least one order of magnitude larger than the number of particles used in the present  $N$ -body simulations, and therefore we expect that the Fokker-Planck model should work well for them.

### 5.3. The mass function

At the start of each calculation the mass function is independent of the distance to the cluster center. Mass loss by stellar evolution and mass segregation due to the dynamical evolution of the star cluster cause the global mass function as well as the local mass function to change with time. After some time the mass function becomes noticeably a function of the distance to the cluster center.

Figure 5 shows the mass function for the  $N$ -body and the Fokker-Planck calculations for the model with  $W_0 = 7$ ,  $\alpha = 2.5$  and family 1 at the age of 10 Gyr. At this moment the clusters has lost about 60% of its initial mass (see Fig. 2c). The differences between the global mass-functions of the  $N$ -body model and of the Fokker-Planck model are negligible. Even the partial mass functions for the main-sequence stars and for the compact objects (white dwarfs and neutron stars) agree excellently. At an age of 10 Gyr the mass function for the main-sequence stars is somewhat flatter than the initial mass function, but the shape of the mass function is still well represented by a single power-law. Also for some other initial models we compared the mass functions at  $t = 10$  Gyr between Fokker-Planck and  $N$ -body models, and found good agreement in all cases.

## 6. Fokker-Planck Survey Results

In this section we present the results of our anisotropic Fokker-Planck calculations in which escaping stars are removed instantaneously from the cluster. These calculations give lower limits to the lifetimes of the clusters (see TPZ). We use the same stellar evolution model as CW in the survey simulations.

Table 3 summarizes the survey results (Aa models) and compares them with the results obtained by CW (their Table 5). Following CW, the destiny of the cluster is classified as ‘C’ for core collapse or ‘D’ for disruption. The mass of the cluster  $M_{\text{end}}$  (in units of the initial mass) and the time  $t_{\text{end}}$  (in Gyr) at the moment we stop the calculations (resulting in C or D) are listed in Table 3. The listed end time for collapsing clusters means the moment of core collapse. These clusters will survive beyond the core collapse, but their post-collapse evolution is not followed in our calculations.

The disruption time as well as the mass at that instant are rather ill defined in Fokker-Planck calculations. By definition a cluster ceases to exist (disrupts) at the moment  $M = 0$ . However Fokker-Planck calculations usually break earlier. Mass loss often accelerates rapidly before the moment the cluster ceases to exist (see Fig. 6). In such a case the Fokker-Planck model fails to find the self-consistent solution of the Poisson equation, and breaks (see CW, § VIIa). CW identified this moment as disruption

time. This may be associated with the moment when the cluster loses dynamical equilibrium (Fukushige & Heggie 1995). CW’s definition, however, is not free from ambiguity particularly for the mass at disruption, since the above-mentioned mass-loss acceleration is related to the breaking of numerical calculations.

For clusters that dissolve we continued the calculations until the mass evolution curves start to bend downwards very rapidly (see Figure 6). We define  $t_{\text{vert}}$  as the moment when the mass loss rate becomes virtually infinite. Then, however, the mass at  $t_{\text{vert}}$  is not well defined. Therefore, for convenience, we decided to take  $t_{\text{end}} = 0.99t_{\text{vert}}$  as the disruption time, and then  $M_{\text{end}} = M(t_{\text{end}})$ . We confirmed by eye that the point  $(t_{\text{end}}, M_{\text{end}})$  determined by the above definition corresponds to the “turn-off point” of the mass evolution curve.

### 6.1. The total mass and the concentration as a function of time

Figure 6 shows the evolution of the total mass for all the initial models. The circles plotted at the ends of some of the lines indicate the moments when those clusters experience core collapse. The destiny of the clusters is determined by the initial conditions ( $W_0$ ,  $\alpha$ , and  $F_{\text{CW}}$ ). The early evolution is strongly affected by the choice of  $W_0$  and  $\alpha$ , and in less extent by the initial relaxation time, simply because the latter requires more time to affect the dynamics of the stellar system. The lifetimes of the clusters which are disrupted within  $\sim 1$  Gyr, for example, are almost independent of the initial relaxation time. The evolution of these clusters is mainly driven by stellar mass loss. This causes the clusters to expand after which the Galaxy gobbles up the clusters. Core collapse occurs only in some long-lived ( $> 3$  Gyr) clusters. For these clusters the mass loss rate gradually decreases with time (see also Portegies Zwart et al. 1998).

Figure 7 shows the evolution of the concentration parameter  $c$ , which we define by (cf. King 1966)

$$c \equiv \log_{10} \frac{r_t}{r_c}. \quad (15)$$

Here the core radius  $r_c$  is

$$r_c \equiv \left( \frac{3v_{\text{m0}}^2}{4\pi G\rho_0} \right)^{1/2}, \quad (16)$$

where  $\rho_0$  is the central density and  $v_{\text{m0}}$  is the density-weighted velocity dispersion in the cluster center. Note that this core radius  $r_c$  and the King core radius (King 1966) are not identical even for single-mass systems, since the central velocity dispersion is not used in the definition of the King radius. The two quantities get closer for more concentrated (higher  $W_0$ ) clusters (cf. Binney & Tremaine 1987, p. 235).

In some cases (for  $W_0 = 7$ ,  $\alpha = 1.5$  of all the families, and for  $W_0 = 1$ ,  $\alpha = 3.5$  of family 1) the cluster experiences core collapse after almost all ( $\sim 99\%$ ) of the initial mass is lost. We identify these clusters as collapsing clusters, because the concentration  $c$  rapidly increases at the final epochs (see Fig. 7). If the initial mass of a cluster is relatively small (e.g.  $M_0 \lesssim 10^4 M_\odot$ ), the definite evidence of core collapse will be very hard to observe, since the number of stars in the core will become too small (e.g.  $N_{\text{core}} \lesssim 10$ ). Deep core collapse in such systems can easily be prevented by the formation of binaries by three-body processes or by burning primordial binaries. Such processes are more effective in small  $N$  clusters.

For  $W_0 = 7$ ,  $\alpha = 1.5$ , irrespective of the families, the clusters have very small masses (compared to their initial masses) around  $t=10$  Gyr. This implies that they may be observed at present as tiny globular clusters or as old open clusters (see § 7.4).

For all the models with  $\alpha = 1.5$ , mass loss due to stellar evolution causes the concentration to decrease

with time before core collapse occurs. For  $\alpha = 2.5$  and  $3.5$ , the concentration does not decrease so much but stays almost constant. If, at any time, the concentration becomes smaller than  $c \approx 0.4$  (compare with  $c = 0.58$  for the  $W_0 = 1$  King model), the cluster quickly dissolves. As CW pointed out (see their section VIIc), the (scaled) density profiles just before disruption are always similar regardless of initial models.

## 6.2. Comparison with Chernoff & Weinberg (1990)

### 6.2.1. Clusters that disrupt

All our clusters of model Aa live longer than those of CW for the same initial conditions. The largest (relative) discrepancy is about a factor of ten which is found for  $(W_0, \alpha) = (1, 2.5)$  and  $(3, 2.5)$ . For the models with  $(W_0, \alpha) = (1, 1.5)$  and  $(3, 1.5)$ , the discrepancy is about a factor of two. In the latter models the mass functions are very flat and the potentials are shallow, and thus stellar mass loss alone is enough to disrupt these clusters. It is therefore not surprising that even the Aa models cannot live so long compared with the CW models. The disruption time hardly depends on the initial relaxation time for those clusters which disrupt within  $\sim 1\%$  of the half-mass relaxation time.

Table 4 compares our Ae and Aa models with CW’s models for family 1. In addition to the data already given in Table 3,  $t_{\text{end}}$  and  $M_{\text{end}}$ , two new quantities,  $t(M_{\text{end}, \text{CW}})$  and  $M(t_{\text{end}, \text{CW}})$ , are presented. Here  $M_{\text{end}, \text{CW}}$  and  $t_{\text{end}, \text{CW}}$  denote the final mass and time, respectively, of each of CW’s models which are given in Table 3. These two quantities are particularly useful for comparing different models for disrupted clusters.

The energy criterion for the tidal boundary is used for the CW models as well as for the Ae models. The Ae models are in this sense in between the CW and Aa models. Comparison with the Ae models helps us to understand how the apocenter criterion affects the results. The Ae models lose mass faster than the Aa models in all the cases shown in Table 4, simply because the energy criterion introduces a larger escape region in phase space than the apocenter criterion (Takahashi et al. 1997; TPZ). The difference between the CW and Ae models is rather small in all cases. For each set of initial conditions the two models have the same destiny, disruption or collapse. The difference in the disruption time is within a factor of two, and that in  $t(M_{\text{end}, \text{CW}})$  is even smaller. We therefore conclude that the introduction of the apocenter criterion plays the most important role in extending the cluster lifetime.

For  $(W_0, \alpha) = (1, 2.5)$  and  $(3, 2.5)$  we find large differences between the CW and Aa models not only in  $t_{\text{end}}$  and  $M_{\text{end}}$  but also in  $t(M_{\text{end}, \text{CW}})$  and  $t(t_{\text{end}, \text{CW}})$ . This assures that the discrepancy between the two models are not merely due to differences in the definitions of the disruption time and mass. The clusters survive beyond the disruption times given by CW, which is also supported by  $N$ -body simulations (TPZ; § 5).

### 6.2.2. Clusters that collapse

About half (seventeen) of the clusters calculated with Aa models experience core collapse, while in the calculations of CW less than 30% (ten) of the clusters experience core collapse. This means that seven of the models of CW are disrupted while the corresponding Aa models experience core collapse. In these Aa models core collapse occurs much later than the disruption time of the CW models; a too high rate of mass loss in the CW models disrupts the clusters too quickly.

All the clusters which experience core collapse according to CW do experience core collapse according to our calculations also. Core collapse occurs after two-body relaxation starts to dominate the evolution of the clusters, i.e.; when stellar-evolution mass loss has sufficiently decreased. Since CW’s models generally overestimate the rate of mass loss, all models that finally develop a collapsed core according to their calculations experience core collapse in our calculations too.

For  $(W_0, \alpha) = (7, 2.5)$  and  $(7, 3.5)$  of all the families, both the models of CW and our Aa models experience core collapse. For these models, the moment of core collapse approximately scales with the initial relaxation time. This indicates that their evolution is dominated by two-body relaxation, not by stellar evolution. In those cases, the differences in the moment of core collapse between CW and Aa models are less than 10 %.

The introduction of anisotropy into the models itself does not have very significant effects on the moment of core collapse (see Takahashi 1995; Takahashi et al. 1997). Core collapse proceeds almost independently of the outer parts of the cluster and the anisotropy in the core is always small. The difference between the energy and apocenter criteria affects mass loss from the tidal boundary, and the mass loss affects core collapse time by reducing the relaxation time. But the effect of the mass loss on core collapse time is only significant for low-concentration clusters which lose a substantial fraction of their mass before collapse (cf. Quinlan 1996).

In addition, when mass loss proceeds slowly, on the relaxation time scale, the difference between the apocenter criterion and the energy criterion is less important than when mass loss proceeds more rapidly driven by stellar evolution. The stars which exit in a region lying between the boundary of the energy criterion and that of the apocenter criterion in phase space (see, Takahashi et al. 1997, Fig. 1; or TPZ, Fig. 1) are responsible for slower mass loss in apocenter-criterion models. These stars diffuse over the tidal boundary on a time scale of the order of the relaxation time. If mass loss by stellar evolution is ineffective and the cluster evolves slowly on the relaxation time scale the difference between apocenter- and energy-criterion models will be small (cf. Takahashi et al. 1997). On the other hand, if the cluster loses mass rapidly due to stellar evolution compared with the relaxation time scale, the above-mentioned phase-space region will play an important role as a mass reservoir.

We therefore conclude that the moment of core collapse is correctly calculated with isotropic Fokker-Planck models as well as with anisotropic Fokker-Planck models as long as the cluster is relaxation-dominated.

Figure 8 gives a graphical representation of Table 3 for family 1. The largest discrepancies occur around a boundary which separates disrupted clusters and collapsing clusters; the disrupted clusters are on the lower left region and the collapsing clusters are on the upper right region in this figure.

For  $W_0 = 3$  and  $\alpha = 3.5$  of family 1 and 2, the differences in the collapse time between isotropic and anisotropic models are rather large. These models are near the separating boundary mentioned above; the CW models of family 1 and 2 collapse but those of family 3 and 4 dissolve. In such cases, even a small difference in the mass loss rate may cause a large difference in the fate of the cluster.

### 6.3. Fokker-Planck Survey Results for $N = 3 \times 10^5$

Real star clusters contain a finite number of stars, typically  $N \sim 10^5 - 10^6$ . It is not clear whether this number is large enough to be treated as infinite, though it is usually assumed in Fokker-Planck calculations.

For example, it is not clear whether the instantaneous escape condition, which is valid for  $N \rightarrow \infty$  and is adopted in our survey simulations, is a good approximation for typical globular clusters. To test the effect of a finite crossing-time, we performed a series of calculations by using the crossing-time removal condition, Eq. (3), with  $N = 3 \times 10^5$ .

Figure 9 presents the mass evolution for models of family 4 with  $N = 3 \times 10^5$  initially. Family 4 has the largest relaxation time and thus has the largest crossing time for fixed  $N$ . The initial total masses of these models are  $7.3 \times 10^5 M_\odot$ ,  $3.0 \times 10^5 M_\odot$ , and  $2.0 \times 10^5 M_\odot$ , and the crossing times  $t_{\text{cr}}$  are 0.03 Gyr, 0.06 Gyr, and 0.10 Gyr, for  $\alpha = 1.5, 2.5$ , and  $3.5$ , respectively. These models are compared with the models with the instantaneous escape condition (see Fig. 6).

The relative difference between the models with  $N = 3 \times 10^5$  and those with  $N \rightarrow \infty$  for the clusters which dissolve within a few Gyr is rather large. In these cases the models with  $N = 3 \times 10^5$  live a factor of two or three longer than the  $N \rightarrow \infty$  models. The lifetime of these clusters is comparable to the crossing time. The evolution of these models is therefore very sensitive to the way escapers are removed from the clusters; crossing-time removal or instantaneous removal. For long-lived clusters that survive for a Hubble time the details of how escaping stars are removed become less important; the instantaneous removal condition gives a good approximation for these cases.

## 7. Discussion

### 7.1. The anisotropic Fokker-Planck model

We have shown that our anisotropic Fokker-Planck (Aa) models are in excellent agreement with  $N$ -body models for a wide range of initial conditions. Although expected from theoretical considerations, it is still quite striking that a single value of  $\nu_{\text{esc}}$  suffices to achieve agreement between the very different types of numerical models and over such a wide range of initial conditions. Subtle differences between the Fokker-Planck and  $N$ -body results, however, remain. These are probably due to the greater detail and higher accuracy of the  $N$ -body models compared to the Fokker-Planck models. (The absence of binary formation via three-body processes in the Fokker-Planck models may also play a role here.) In some cases, the relatively simplistic implementation of the tidal field via a cut-off radius causes a somewhat peculiar behavior in the  $N$ -body models (see § 7.2). Fokker-Planck models lose their credibility when the time scale for mass loss becomes comparable to the dynamical time scale, since in that case the assumption of an adiabatic change in the potential is violated.

Concerning the models shown in the present paper, all the Aa models live longer than the isotropic models. However, there are cases where anisotropic models live longer than isotropic models. For example, Takahashi et al. (1997) show the results that, in the absence of stellar evolution, Aa and Ae models evaporate faster than an isotropic model in the tidal field. The shorter lifetime of these anisotropic models is induced by two-body relaxation at the inner regions which causes a quick emergence of elongated-orbit stars in the halo. The apocenters of these stars are frequently outside the tidal radius. Especially when the tidal field is relatively weak mass loss in anisotropic models is quicker than in isotropic models (see Takahashi & Lee 1999 for details).

The apocenter criterion is considered more realistic than the energy criterion, but also this approach has its limitation. The implementation of a spherical cutoff radius instead of a self-consistent tidal field, for example, limits the conditions on which escapers are identified. However, also in a real cluster a

star must pass the tidal radius in order to leave the cluster. The apocenter criterion is therefore an important improvement over the simple energy criterion used in previous Fokker-Planck calculations. The implementation of the apocenter criterion, however, requires anisotropic Fokker-Planck models; isotropic Fokker-Planck models do not contain sufficient information about the stars’ orbits to apply the apocenter criterion. Unfortunately it seems hard to adjust the energy criterion used in isotropic models such that the mass loss rate becomes similar to that for the apocenter criterion. This is because the apocenter criterion causes the cluster’s mass-loss rate to depend on the angular-momentum distribution (anisotropy) of the stars near the tidal boundary, and the anisotropy behaves in a rather complex way: it changes with time, and depends on the mass of the stars and the distance to the cluster center (Takahashi 1997; Takahashi et al. 1997).

## 7.2. Effect of the tidal field

To investigate the effect of the self-consistent tidal field compared with the adopted tidal cut-off, we perform several  $N$ -body calculations with different implementations of the tidal field. The same initial conditions as for the models in Figure 2a are adopted. For each model, calculations are performed ten times using different sets of random numbers with 1024 stars. The results are presented in Figure 10.

The solid line in Figure 10 represents the mean of ten calculations with a simple tidal cut-off (model TCR1, the  $\sigma/2$  deviations from the mean are shown in Figure 2a). The other lines represent the results for the calculations with a self-consistent tidal field. For all the tidal-field models the same tidal force is used but different cut-off (maximum) radii are selected. Stars in the tidal-field models are removed as soon as they go beyond  $r_t$  (model TFR1; the T stands for tidal, F for field and the R stands for the radius, in units of the tidal radius, at which stars are removed from the simulation),  $2r_t$  (model TFR2),  $10r_t$  (model TFR10), or  $100r_t$  (model TFR100) from the cluster center. For computational reasons it is convenient to set a cut-off radius even for the calculations where a tidal field is used. The mass given in Figure 10 is the mass contained in stars which are bound to the cluster.

All the models presented in Figure 10 are indistinguishable for the first one billion years, where mass loss is dominated by stellar evolution. After that, model TCR1 and model TFR1 start to lose mass more rapidly than the other models. This acceleration in mass loss is related to a too sudden removal of escaping stars which is caused by the small cut-off radius. Model TFR1 keeps losing mass at a rate slightly higher than the other tidal-field models. After about 2 Gyr the mass loss rate of model TCR1 becomes smaller than for the models with a tidal field. Not surprisingly, stars are removed more quickly if a tidal field is incorporated and stars are removed at  $r_t$ . Figure 10 shows that an artificial cut-off radius in excess of  $2r_t$  hardly affects the results in the models where a self-consistent tidal field is incorporated.

The Fokker-Planck model with 1K stars (see Figure 2a) loses more mass in the first billion years than the  $N$ -body models (TCR1, TFR1 to TFR100). This difference may be caused by the assumed adiabatic response of the Fokker-Planck models to changes in the potential (Cohn 1979). The cluster loses about 30% of its initial mass within 1 Gyr. Since the initial half-mass crossing time is about 0.5 Gyr, this change in the potential is quite impulsive. In spite of this breakdown of one of the fundamental assumptions in Fokker-Planck models, the agreement with the  $N$ -body model is, except model TFR1, fairly good.

We have demonstrated that  $N$ -body and Fokker-Planck models with the tidal cut-off behave in a similar fashion as  $N$ -body models with the self-consistent tidal field, for one selected set of initial conditions. However, it is not obvious whether tidal cut-off models are always similar to tidal-field models. Giersz &

Heggie (1997) also investigated the difference between these two kinds of  $N$ -body models. They concluded that the mass evolution is not much affected by the difference between the two implementations of the tidal boundary conditions. We like to encourage further investigations on this issue.

### 7.3. Comparison with similar $N$ -body surveys by other authors

Recently Aarseth & Heggie (1998) investigated the time scaling of  $N$ -body models with respect to the number of stars. They incorporated the Galactic tidal field in the same way as Fukushige & Heggie (1995) did. The same stellar evolution tracks as used by CW were adopted.

Aarseth & Heggie (1998) introduced “variable time scaling” which couples the stellar evolution time scale to the time scale on which the star cluster evolves dynamically. During the early stages of the evolution of the cluster, when the effect of stellar evolution is dominant, time scaling based on the crossing time is applied. At later stages, when two-body relaxation becomes dominant, the relaxation time is used for time scaling. This variable time scaling has a qualitative physical basis, but there remains uncertainty in when and how to change from one scaling to another.

Using the variable time scaling Aarseth & Heggie (1998) find good agreement between their  $N$ -body calculations and the Fokker-Planck calculations of CW for those clusters that survive long enough for their evolution to become dominated by two-body relaxation. For quickly disrupted clusters, the models of CW live too short compared to the models of Aarseth & Heggie (1998). These conclusions are qualitatively consistent with our conclusions on the comparison between our Fokker-Planck models and the CW models. A detailed comparison between Aarseth & Heggie’s (1998)  $N$ -body models and our Fokker-Planck models is complicated by the difference in the implementation of the tidal field.

In Table 5 our Aa models are compared with the  $N$ -body results of Aarseth & Heggie (1998, Table 3) as well as those of Fukushige & Heggie (1995, Table 3) for family 1, in terms of core collapse time and mass, and disruption time and mass. The models of the former authors are denoted by “AH”, and those of the latter by “FH”. A number associated with each of these model names indicates the galactocentric distance  $R_g$  (in kpc) at which that model is placed. The initial cluster mass is  $5.45 \times 10^4 M_\odot$  at  $\sim 10$  kpc, and  $1.49 \times 10^5 M_\odot$  at  $\sim 4$  kpc. The Aa models use the instantaneous escape condition and their evolution is, within one family, independent of  $R_g$ . Fukushige & Heggie (1995) use fixed time scaling based on the crossing time, which is considered to be appropriate for the early evolution of clusters. Table 5 shows only those models for which they obtain definite lifetimes.

The disruption time and mass,  $t_{\text{dis}}$  and  $M_{\text{dis}}$ , are listed in Table 5. The  $N$ -body models disrupt at the moment the mass has dropped to zero, but, as we discussed above, the Fokker-Planck calculations usually stop well before the mass goes to zero. Therefore we should be aware that  $t_{\text{dis}}$  for the  $N$ -body models and that for Fokker-Planck models do not have exactly the same meaning.

For  $(W_0, \alpha) = (1, 2.5)$  and  $(3, 2.5)$  the results of CW are very different from those of FH and AH, but our Aa models are consistent with the results of FH and AH. For models with the flat initial mass function of  $(W_0, \alpha) = (1, 1.5)$  and  $(3, 1.5)$ , the results of CW deviate largely from the calculations of FH and AH. For these cases, the lifetimes of our Aa models ( $\sim 0.02$  Gyr) are about twice as long as those of CW’s models, but they are still shorter than the lifetimes of the models of FH and AH by a factor of a few. This difference will be reduced when the crossing-time removal condition is applied for Fokker-Planck models. As discussed in § 6.3, for such short-lived clusters with small  $N$ , the instantaneous removal condition gives somewhat



too short lifetimes (see Fig. 9).

The Aa models (as well as CW’s models) with  $(W_0, \alpha) = (7, 2.5)$  and  $(7, 3.5)$  experience core collapse at about the same time and at about the same cluster mass as the models of AH. For  $(W_0, \alpha) = (1, 3.5)$  and  $(7, 1.5)$  the Aa models collapse while the  $N$ -body models do not. The masses of these Aa models at the moment of core collapse, however, are only  $\sim 0.01M_0$ , and thus it is not surprising that the core collapse does not occur in the  $N$ -body systems comprising initially of only a few thousand particles.

#### 7.4. Comparison with the observations

For a better comparison, all our calculations are performed with the same initial conditions as adopted by CW. These initial conditions, however, are probably not the best choice for real globular clusters. Recent observations have revealed that mass functions are ill represented by a single power-law (e.g., Scalo 1986; Kroupa et al. 1990) and that the lower stellar mass limit should be  $\lesssim 0.1M_\odot$  (e.g, De Marchi & Paresce 1995a; 1995b; Marconi et al. 1998; see also Chernoff 1993). Another uncertainty, which may seriously affect the simulation results, is the initial compactness of star clusters. The King models from which we selected the initial density profiles may not be the best choice for the initial density profiles for tidally-truncated star clusters (Heggie & Ramamani 1995). It is not even clear whether real globular clusters were born filling up their tidal lobes. Initial under-filling of the tidal lobe may extend the cluster lifetime considerably. Regardless of these uncertainties in the initial conditions, it will be still worthwhile to discuss some implications for the observed population of globular clusters.

Our calculations indicate that clusters which are observed in a state of core collapse at present must have been born fairly concentrated, otherwise core collapse would not be occurring within the age of the Universe. At core collapse most of the models have lost  $\gtrsim 50\%$  of their initial mass. This indicates that observed globular clusters in a state of core collapse were born with a high concentration and considerably more massive than today’s mass.

All the clusters with a concentration parameter  $c \approx 1$  at  $t \approx 10$  Gyr appear to be in a local minimum in concentration. These clusters recover their concentrations later as core collapse follows. A cluster which reaches a concentration of  $c \approx 0.4$  at any time evaporates quickly thereafter. The least concentrated globular clusters in our Galaxy have a King concentration parameter of  $c_{\text{King}} \approx 0.5$  (Trager et al. 1993). This is consistent with our findings.<sup>4</sup>

According to our survey most of globular clusters with a rather flat initial mass function ( $\alpha = 1.5$ ) disrupt within a Hubble time. This indicates that the majority of the present-day clusters probably had steeper initial mass functions. However, we cannot exclude the possibility that some of the globular clusters were born with an initial mass function of  $\alpha \sim 1.5$  but have still survived owing to the initial high concentration. For example, the model with  $W_0 = 7$ ,  $\alpha = 1.5$  and family 3 loses about 99% of its initial mass and has still a high concentration at 12 Gyr (see Figs. 6 and 7). The old open cluster Berkeley 17 has similar characteristics as this model, as we show below.

Phelps (1997) derives an age for Berkeley 17 of 10 Gyr to 13 Gyr (but Carraro et al., 1999, estimates an age of  $9 \pm 1$  Gyr), a distance to the Galactic center of  $R_g = 11$  kpc, a size of  $\sim 5$  pc, and a total mass in

---

<sup>4</sup>Note, however, that  $c_{\text{King}}$  is not identical to the  $c$  (see § 6) and that the one- $\sigma$  error in the observed  $c_{\text{King}}$  is about 0.2 (Trager et al. 1993).

visible stars of about  $400 M_{\odot}$ .

The core of the model with  $W_0 = 7$ ,  $\alpha = 1.5$  and family 3 collapses at an age of 12 Gyr. At this moment the total mass is only 1.3% of its initial mass (see Table 3). Substitution of  $R_g = 11$  kpc and  $v_g = 220$  km/s into Eq. (10) results in an initial mass of  $M_0 \approx 2.3 \times 10^5 M_{\odot}$ . At the moment of core collapse the cluster has then a mass of  $\sim 3000 M_{\odot}$  and the half-mass radius of  $\sim 4$  pc. The majority of this mass is hidden in stellar remnants, i.e.:  $\sim 900 M_{\odot}$  in neutron stars and  $\sim 1700 M_{\odot}$  in white dwarfs, and only  $\sim 400 M_{\odot}$  is in main-sequence stars (see also Heggie & Hut 1996; Vesperini & Heggie 1997 for dark remnants in globular clusters). This model cluster looks similar to Berkeley 17 in the size and luminous mass.

We note that the fraction of neutron stars in our models is overestimated, since many are likely to escape from the cluster by a “kick” at the time of a supernova explosion. An intrinsic asymmetry in the supernova is believed to give neutron stars a kick velocity which is generally much higher than the escape velocity from the cluster (Drukier 1996; Portegies Zwart & van den Heuvel 1999). This effect is not taken into account in our calculations.

Figure 11 shows the global mass function for the model with  $W_0 = 7$ ,  $\alpha = 1.5$ , and family 3, at  $t = 12$  Gyr. The filled circles and the open circles represent the mass functions for the white dwarfs and for the main-sequence stars, respectively. The mass function for the main-sequence stars peaks at  $m \sim 0.8 M_{\odot}$ . The stars with  $m \gtrsim 0.8 M_{\odot}$  have evolved off the main-sequence. The peculiar shape of the main-sequence mass function for  $m \lesssim 0.8 M_{\odot}$ , which decreases with decreasing  $m$ , is the result of the preferential loss of low mass stars through the tidal boundary; high mass stars are more centrally concentrated than low mass stars due to mass segregation and therefore have less chance to escape. In general the global mass function becomes flatter as the cluster loses mass (e.g. Vesperini & Heggie 1997). However, it is rare to find such an inverted global mass function as is shown in Fig. 11 in our surveyed models. Such a mass function only appears in clusters which have lost  $\gtrsim 99\%$  of their initial mass on the relaxation time scale. These “remnant” clusters were formerly the cores of more massive clusters. High mass stars are over-abundant in such cores as a result of mass segregation.

The mass function of the globular cluster NGC 6712 around the half-light radius also peaks near  $0.75 M_{\odot}$  (De Marchi et al. 1999), and looks similar to the mass function shown in Fig. 11. (Although Fig. 11 shows the global mass function, the local mass function at the half-mass radius is similar to that.)

De Marchi et al. (1999) interpreted the observed inverted mass function as evidence for severe tidal disruption, which is consistent with the above model. Thus we suspect that NGC 6712 was born far more massive than what it is today. With the current mass of  $\sim 10^5 M_{\odot}$  (Pryor & Meylan 1993), its initial mass would be  $\sim 10^7 M_{\odot}$ , if that model is applied. However, this prediction of the initial mass is rather uncertain quantitatively, because our survey is limited in many respects. The range of initial conditions covered by our survey is still limited, as mentioned above. Further we assume a steady tidal field. The orbit of NGC 6712 is, in fact, likely to be very eccentric; the cluster is presently at  $R_g = 3.5$  kpc, but the minimum and maximum galactocentric distances are predicted to be about 0.3 kpc and 7 kpc, respectively (Dauphole et al. 1996). Therefore, bulge and disk shocks (see Gnedin & Ostriker 1997; Murali & Weinberg 1997; and references therein) have probably affected the mass evolution of this cluster considerably, as pointed out by De Marchi et al. (1999).

Since we argued above that Berkeley 17 may be represented by the model shown in Fig. 11, it will be interesting to observe the mass function of Berkeley 17 down to very low mass stars.

## 8. Conclusions

We have investigated the evolution of star clusters including the effects of the tidal field of the parent galaxy and mass loss from stellar evolution by using *anisotropic* Fokker-Planck models as well as *N*-body models. Our new Fokker-Planck models, which include a new implementation of the tidal field, agree much better with *N*-body models than *isotropic* Fokker-Planck models.

The new implementation of the tidal boundary consists of two parts: the apocenter criterion assures that only those stars are removed from the stellar system for which apocenter radius exceeds the tidal radius of the cluster; the crossing-time removal condition prevents escaping stars from being removed in an infinitesimal time step, but keeps them in the stellar system for some time of the order of the crossing-time. The crossing-time removal introduces an additional free parameter,  $\nu_{\text{esc}}$ , to the Fokker-Planck model. We find that a single value of  $\nu_{\text{esc}} = 2.5$  provides good agreement between *N*-body and Fokker-Planck calculations over a wide range of initial conditions. These improvements to the Fokker-Planck model allow us to perform calculations in much wider ranges of parameter space, including varying the number of stars. This opens the possibility to compare Fokker-Planck calculations directly with direct *N*-body calculations.

With the improved Fokker-Planck model we have studied the evolution of globular clusters over a wide range of initial conditions. The surveyed initial parameters are identical to those adopted by CW. Our clusters live generally longer than the isotropic models of CW. The largest differences appear in cases where clusters dissolve promptly in the tidal field before core collapse occurs, except for cases of too prompt dissolution due to too severe mass loss via stellar evolution. For some initial conditions, our models reach core collapse, while the models of CW dissolve. The differences are rather small for long-lived clusters which start with steep mass functions and high concentrations and finally reach core collapse. These findings are consistent with the conclusions of Aarseth & Heggie (1998) who compare their *N*-body models with the models of CW.

About half of the clusters calculated in our survey are disrupted within 10 Gyr. Only four of our 36 samples experience core collapse within 10 Gyr, and two of the four have lost more than 99% of their mass at the moment of core collapse. This suggests that the range of the initial conditions with which clusters reach core collapse within the age of the Universe is rather small in our survey. On the other hand, about 20% of the known Galactic globular clusters are classified as post-collapse clusters (Djorgovski & King 1986; Chernoff & Djorgovski 1989; Trager et al. 1993). These post-collapse clusters might have been born with initial conditions that are preferable for core collapse at  $\sim 10$  Gyr, e.g.,  $\alpha = 2.5$  and  $3 < W_0 \lesssim 7$ . However it should be noted that not all of possible initial conditions of real globular clusters are covered by our (and CW's) survey. In particular the adopted initial mass functions are probably not the best choice.

In the survey we find a few peculiar models which have very small masses ( $\sim 1\%$  of the initial mass) but are well concentrated at  $\sim 10$  Gyr. Such clusters happen to be classified as old open clusters, like Berkeley 17, rather than as globular clusters, depending on their luminosities, appearances, and positions relative to the Galactic disk. The present-day global mass functions of these model clusters are also peculiar in the sense that they decrease with decreasing stellar mass. A similar inverted mass function was observed in the globular cluster NGC 6712 by De Marchi et al. (1999). This indicates that NGC 6712 might have lost a very large fraction of its initial mass, if the observed mass function is really close to the global mass function and does not only reflect a peculiarity of the initial mass function of the cluster.

Clusters which lose  $\gtrsim 50\%$  of their initial mass in a very short time scale may still survive for a long time. The principle that losing more than a half of the initial mass of a cluster inevitably results in

disruption is based on the virial theorem and on the assumption of impulsive mass loss (Hills 1980). For the initial conditions of  $W_0 = 7$ ,  $\alpha = 1.5$ , and family 4, more than half the cluster mass is lost within a few half-mass crossing times (see Fig. 2e). But, in fact, still the cluster survives for more than ten billion years and finally experiences core collapse.

Comparison between  $N$ -body calculations with various implementations of the galactic tidal field and the cut-off boundary condition indicates that there may be a significant population of stars which are trapped outside the tidal radius of the cluster but are still bound to the stellar system.

We are grateful to Piet Hut, Junichiro Makino, and Steve McMillan for many discussions and software development. We also thank Haldan Cohn, Toshiyuki Fukushige, and Douglas Heggie for enlightening discussions. SPZ is grateful to University of Tokyo for its hospitality and for the use of the fabulous GRAPE system. We wish to express our special thanks to the anonymous referee for constructive comments which led us to further careful examinations of the results. This work was supported in part by the Research for the Future Program of Japan Society for the Promotion of Science (JSPS-RFTP97P01102), and by NASA through Hubble Fellowship grant HF-01112.01-98A awarded (to SPZ) by the Space Telescope Science Institute, which is operated by the Association of Universities for Research in Astronomy, Inc., for NASA under contract NAS 5-26555.

## REFERENCES

- Aarseth, S. J., & Heggie, D. C. 1998, *MNRAS*, 297, 794
- Binney, J., & Tremaine, S. 1987, *Galactic Dynamics* (Princeton University Press, Princeton)
- Carraro, G., Vallenari, A., Girardi, L., & Richichi, A., 1999, *A&A*, 343, 825
- Chernoff, D. F. 1993, in *Structure and Dynamics of Globular Clusters*, ASP Conference Series Vol. 50, ed. S. G. Djorgovski & G. Meylan (San Francisco: ASP), 245
- Chernoff, D. F., & Djorgovski, S. 1989, *ApJ*, 339, 904
- Chernoff, D. F., & Weinberg, M. D. 1990, *ApJ*, 351, 121 (CW)
- Cohn, H. 1979, *ApJ*, 234, 1036
- Cohn, H. 1980, *ApJ*, 242, 765
- Dauphole, B., Geffert, M., Colin, J., Ducourant, C., Odenkirchen, M., & Tucholke, H. J. 1996, *A&A*, 313, 119
- De Marchi, G., Leibundgut, B., Paresce, F., & Pulone, L. 1999, *A&A*, 343, L9
- De Marchi, G., & Paresce, F. 1995a, *A&A*, 304, 202
- De Marchi, G., & Paresce, F. 1995b, *A&A*, 304, 211
- Djorgovski, S., & King, I. R. 1986, *ApJ*, 305, L61
- Drukier, G. A., 1995, *ApJS*, 100, 347

- Drukier, G. A., 1996, MNRAS, 280, 498
- Drukier, G. A., Cohn, H. N., Lugger, P. M., & Yong, H. 1999, ApJ, 518, 233
- Fukushige, T., & Heggie, D. C. 1995, MNRAS, 276, 206
- Giersz, M. 1998, MNRAS, 298, 1239
- Giersz, M., & Heggie, D. C. 1994a, MNRAS, 268, 257
- Giersz, M., & Heggie, D. C. 1994b, MNRAS, 270, 29
- Giersz, M., & Heggie, D. C. 1997, MNRAS, 286, 709
- Giersz, M., & Spurzem, R. 1994, MNRAS, 269, 241
- Gnedin, O., & Ostriker, J. P. 1997, ApJ, 474, 223
- Heggie, D. C., Giersz, M., Spurzem, R., & Takahashi, K. 1999, in Highlights of Astronomy, Vol. 11, ed. J. Andersen
- Heggie, D. C., & Hut, P. 1996, in IAU Symp. 174, Dynamical Evolution of Star Clusters, ed. P. Hut & J. Makino (Dordrecht: Kluwer), 303
- Heggie, D. C., & Ramamani, N., 1995, MNRAS 272, 317
- Hills, J. G. 1980, ApJ, 225, 986
- Hut, P. 1994, in IAU Symp. 165, Compact stars in binaries, ed. J. van Paradijs and E. P. J. van den Heuvel & E. Kuulkers (Kluwer), 377
- Hut, P., Makino, J., & McMillan, S. 1995, ApJ, 443, 93
- Janes, K. A., & Phelps, R. L. 1994, AJ, 108, 1773
- King, I. 1966, AJ, 71, 64.
- Kroupa, P. Tout, C. A., & Gilmore, G. 1990 MNRAS, 244, 76
- Lee, H. M., Goodman, J. 1995, ApJ, 443, 109
- Lee, H. M., & Ostriker, J. P. 1987, ApJ, 322, 123
- Makino, J., & Aarseth, S. J. 1992, PASJ, 44, 141
- Makino, J., Taiji, M., Ebisuzaki, T., & Sugimoto, D. 1997, ApJ, 480, 432
- Makino, J. 1991, ApJ 369, 200
- Marconi, G., Buonanno, R., Carretta, E., Ferraro, F. R., Fusi Pecci, F., Montegriffo, P., De Marchi, G., Paresce, F., & Laget, M. 1998, MNRAS, 293, 479
- McMillan, S. L. W. 1986a, ApJ 307, 126
- McMillan, S. L. W. 1986b, ApJ 306, 552
- McMillan, S. L. W., Hut, P. 1996 ApJ 467, 348

- Meylan, G., & Heggie, D. C. 1997, *A&A Rev.* 8,1
- Murali, C., & Weinberg, M. D. 1997, *MNRAS*, 291, 717
- Phelps, R. L. 1997, *ApJ*, 483, 826
- Portegies Zwart, S. F., & Verbunt, F. 1996, *A&A*, 309 179
- Portegies Zwart, S. F., & Yungelson, L. 1998, *A&A*, 332, 173
- Portegies Zwart, S. F., Hut, P., Makino, J., & McMillan, S. L. W. 1998, *A&A*, 337, 363
- Portegies Zwart S.F., van den Heuvel E. P. J., 1999, *New Astron.*, 4, 355
- Pryor, C., & Meylan, G. 1993, in *Structure and Dynamics of Globular Clusters*, ASP Conference Series Vol. 50, ed. S. G. Djorgovski & G. Meylan (San Francisco: ASP), p357
- Quinlan, G. D., 1996, *New Astron.*, 1, 255
- Ross, D. J., Mennim, A., & Heggie, D. C. 1997, *MNRAS*, 284, 811
- Scalo, J. M. 1986, *Fund. of Cosm. Phys.*, 11, 1
- Spitzer, L. Jr. 1987, *Dynamical Evolution of Globular Clusters* (Princeton University Press, Princeton)
- Spurzem, R., & Takahashi, K. 1995, *MNRAS*, 272, 772
- Takahashi, K. 1995, *PASJ*, 47, 561
- Takahashi, K. 1996, *PASJ*, 48, 691
- Takahashi, K. 1997, *PASJ*, 49, 547
- Takahashi, K., & Lee, H. M., 1999, submitted to *MNRAS* (astro-ph/9909006)
- Takahashi, K., Lee, H. M., & Inagaki, S. 1997, *MNRAS*, 292, 331
- Takahashi, K., & Portegies Zwart, S. F. 1998, *ApJ*, 503, L49 (TPZ)
- Trager, S. C., Djorgovski, S., & King, I. R. 1993, in *Structure and Dynamics of Globular Clusters*, ASP Conference Series Vol. 50, ed. S. G. Djorgovski & G. Meylan (San Francisco: ASP), 347
- Vesperini, E., & Heggie, D. C. 1997, *MNRAS*, 289, 898

Table 1. Stellar evolution models.

$m_{\text{ini}}/M_{\odot}$	$\log(t_{\text{MS}}/\text{yr})$		$m_{\text{fin}}/M_{\odot}$	
	CW	SeBa	CW	SeBa
0.40	11.3	11.3	0.40	0.40
0.60	10.7	10.8	0.49	0.52
0.80	10.2	10.4	0.54	0.56
1.00	9.89	10.0	0.58	0.59
2.00	8.80	9.02	0.80	0.69
4.00	7.95	8.29	1.24	0.80
8.00	7.34	7.64	0.00	1.33
15.00	6.93	7.14	1.40	1.34

Table 2. Families.

Family	$F_{\text{CW}}$	$t_{\text{rlx,CW}}/\text{Gyr}$	$(\langle m \rangle / M_{\odot})(t_{\text{rh}}/\text{Gyr})$		
			$W_{\odot} = 1$	$W_{\odot} = 3$	$W_{\odot} = 7$
1	$5.00 \times 10^4$	128	3.4	2.5	0.7
2	$1.32 \times 10^5$	339	9.0	6.5	1.9
3	$2.25 \times 10^5$	577	15.4	11.0	3.2
4	$5.93 \times 10^5$	1522	40.6	29.1	8.3

<sup>a</sup>The mean stellar mass  $\langle m \rangle = 2.45M_{\odot}$ ,  $1.01M_{\odot}$ , and  $0.66M_{\odot}$ , for  $\alpha = 1.5$ , 2.5, and 3.5, respectively.

Table 3. Survey results.

$W_0$	$\alpha$	Family							
		1		2		3		4	
		CW	Aa	CW	Aa	CW	Aa	CW	Aa
1	1.5	D	D	D	D	D	D	D	D
		$9.2 \times 10^{-3}$	0.017	$9.4 \times 10^{-3}$	0.018	$9.3 \times 10^{-3}$	0.018	$9.3 \times 10^{-3}$	0.018
	2.5	0.78	0.61	0.78	0.63	0.78	0.63	0.79	0.62
		D	D	D	D	D	D	D	D
		0.034	0.31	0.034	0.32	0.035	0.32	0.034	0.33
	3.5	0.77	0.55	0.77	0.56	0.76	0.56	0.77	0.57
		D	C	D	D	D	D	D	D
		2.5	21.6	2.9	24.0	3.1	28.1	3.2	36.2
		0.64	0.021	0.73	0.27	0.74	0.34	0.76	0.44
3	1.5	D	D	D	D	D	D	D	D
		0.014	0.026	0.014	0.026	0.014	0.026	0.014	0.026
		0.53	0.42	0.55	0.41	0.55	0.41	0.54	0.41
	2.5	D	D	D	D	D	D	D	D
		0.28	2.2	0.29	2.7	0.29	2.9	0.29	3.0
		0.46	0.27	0.47	0.32	0.48	0.34	0.49	0.37
	3.5	C	C	C	C	D	C	D	C
		21.5	32.1	44.4	79.8	42.3	129	43.5	313
		0.078	0.17	0.035	0.14	0.085	0.13	0.28	0.11
7	1.5	D	C	D	C	D	C	D	C
		1.0	3.1	3.0	7.7	4.2	12	5.9	27
		0.022	0.010	$3.3 \times 10^{-3}$	0.012	$8.0 \times 10^{-3}$	0.013	0.023	0.011
	2.5	C	C	C	C	C	C	C	C
		9.6	10.1	22.5	23.8	35.5	37.7	83.1	88.7
		0.26	0.32	0.26	0.32	0.26	0.32	0.25	0.31
	3.5	C	C	C	C	C	C	C	C
		10.5	9.9	31.1	30.9	51.3	53.2	131.3	135
		0.57	0.65	0.51	0.58	0.48	0.55	0.49	0.55

<sup>a</sup> The results of Chernoff & Weinberg (1990, CW) are taken from their Table 5. Aa represents our results for the anisotropic Fokker-Planck models with the apocenter criterion.

<sup>b</sup> The first entry describes the fate of the cluster at the end time of the simulation  $t_{\text{end}}$ : C (core collapse) or D (disruption). The second entry is  $t_{\text{end}}$  in units of  $10^9$  yr. The third entry is the cluster mass at  $t_{\text{end}}$ ,  $M_{\text{end}}$ , in units of the initial mass.



Table 4. Comparison of CW, Ae, and Aa models for family 1.

$W_0$	$\alpha$	Model	Fate	$t_{\text{end}}$ [Gyr]	$M_{\text{end}}$ [ $M_0$ ]	$t(M_{\text{end,CW}})$ [Gyr]	$M(t_{\text{end,CW}})$ [ $M_0$ ]
1	1.5	CW	D	0.0092	0.78	0.0092	0.78
		Ae	D	0.013	0.69	0.012	0.98
		Aa	D	0.017	0.61	0.014	0.98
	2.5	CW	D	0.034	0.77	0.034	0.77
		Ae	D	0.056	0.61	0.046	0.85
		Aa	D	0.31	0.55	0.12	0.89
	3.5	CW	D	2.5	0.64	2.5	0.64
		Ae	D	3.1	0.45	2.3	0.60
		Aa	C	21.6	0.021	6.3	0.82
3	1.5	CW	D	0.014	0.53	0.014	0.53
		Ae	D	0.019	0.49	0.019	0.76
		Aa	D	0.026	0.42	0.025	0.82
	2.5	CW	D	0.28	0.46	0.28	0.46
		Ae	D	0.45	0.38	0.40	0.58
		Aa	D	2.2	0.27	1.5	0.72
	3.5	CW	D	21.5	0.078	21.5	0.078
		Ae	C	23.6	0.097	–	0.14
		Aa	C	32.1	0.17	–	0.37
7	1.5	CW	D	1.0	0.022	1.0	0.022
		Ae	D	1.1	0.030	1.1	0.046
		Aa	C	3.1	0.010	2.7	0.12
	2.5	CW	C	9.6	0.26	9.6	0.26
		Ae	C	9.5	0.27	–	–
		Aa	C	10.1	0.32	–	0.34
	3.5	CW	C	10.5	0.57	10.5	0.57
		Ae	C	9.7	0.61	–	–
		Aa	C	9.9	0.65	–	–

<sup>a</sup>Most of the notation is defined in the notes to Table 3.

<sup>b</sup> Ae represents anisotropic Fokker-Planck models with the energy criterion.

<sup>c</sup> $M_{\text{end,CW}}$  and  $t_{\text{end,CW}}$  denote the end mass and the end time, respectively, of each of the CW models. See text for more details.

Table 5. Comparison with  $N$ -body models of FH and AH for family 1.

$W_0$	$\alpha$	Model	$t_{\text{cc}}$ [Gyr]	$t_{\text{dis}}$ [Gyr]	$M_{\text{cc}}$ [ $M_0$ ]	$M_{\text{dis}}$ [ $M_0$ ]
1	1.5	FH3.7	–	0.076	–	0
		Aa	–	0.017	–	0.61
	2.5	FH4.0	–	0.29	–	0
		Aa	–	0.31	–	0.55
	3.5	FH4.1	–	2.2	–	0
3	1.5	Aa	22	–	0.021	–
		FH3.7	–	0.11	–	0
		AH3.7	–	0.075	–	0
		AH9.2	–	0.12	–	0
		Aa	–	0.026	–	0.42
	2.5	FH4.0	–	0.91	–	0
		AH4.0	–	3.0	–	0
		AH10.0	–	3.4	–	0
	3.5	Aa	–	2.2	–	0.27
		AH4.1	–	>20	–	–
		AH10.4	–	>20	–	–
		Aa	32	–	0.17	–
7	1.5	AH3.7	–	1.2	–	0
		AH9.2	–	3.2	–	0
		Aa	3.1	–	0.010	–
	2.5	AH4.0	13	>20	0.21	–
		AH10.0	11	>20	0.257	–
		Aa	10	–	0.32	–
	3.5	AH4.1	10.4	>20	0.606	–
		AH10.4	10.5	>20	0.62	–
		Aa	9.9	–	0.65	–

<sup>a</sup>Part of the notation is defined in the notes to Table 3.

<sup>b</sup>FH denotes  $N$ -body models of Fukushige & Heggie (1995), and AH denotes  $N$ -body models of Aarseth & Heggie (1998). A number associated with each of these model names indicates the galactocentric distance  $R_g$  (in kpc) at which that model is placed.

<sup>c</sup> $t_{\text{cc}}$  and  $M_{\text{cc}}$  denote the collapse time and mass, respectively.  $t_{\text{dis}}$  and  $M_{\text{dis}}$  denote the disruption time and mass, respectively.

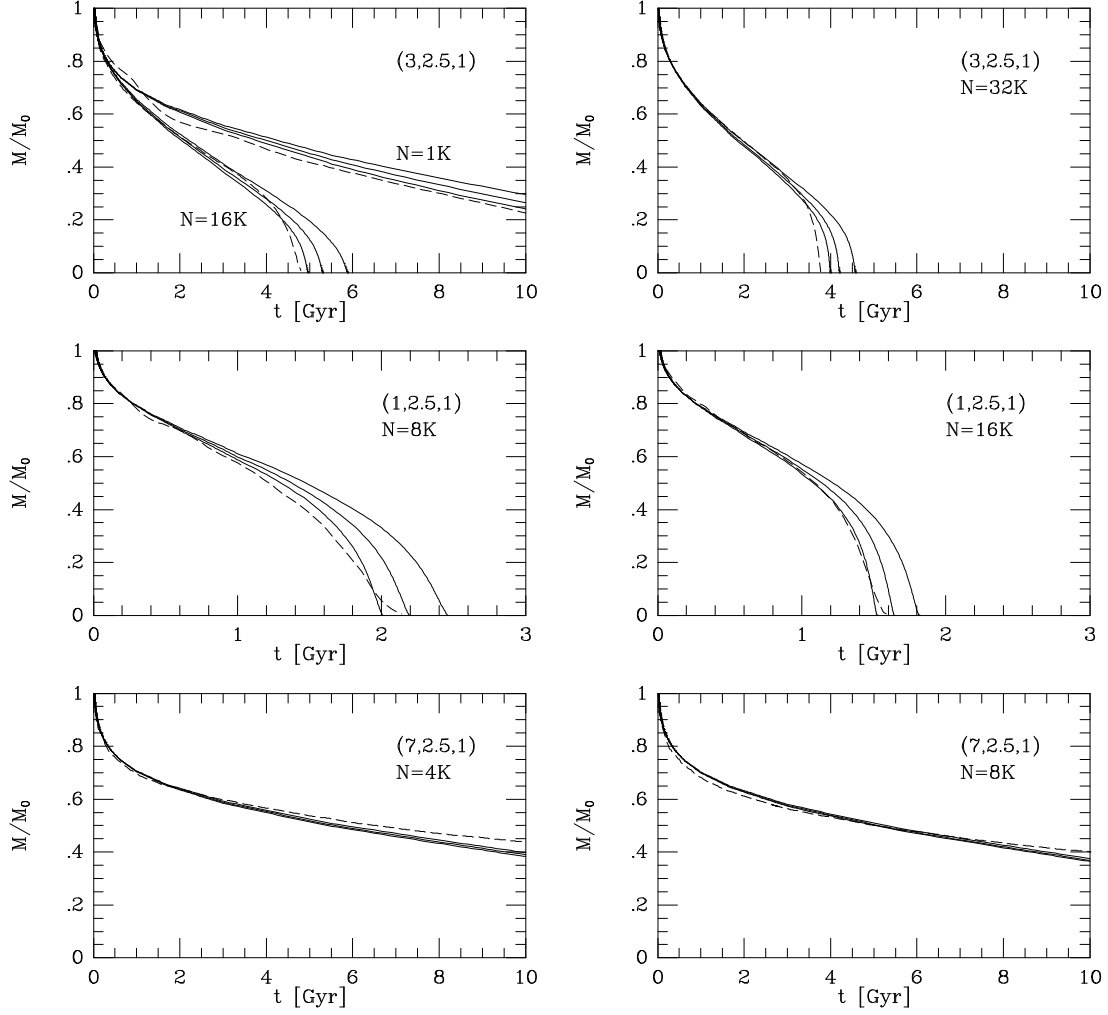


Fig. 1.— Comparison of  $N$ -body models (dashed lines) with Aa Fokker-Planck models with  $\nu_{\text{esc}} = 2, 2.5$ , and 3 (the lower, middle, and upper solid lines, respectively) for the evolution of the total mass. Larger  $\nu_{\text{esc}}$  causes faster mass loss. Top panels: the initial conditions are  $(W_\odot, \alpha, \text{family}) = (3, 2.5, 1)$ . The average of 10 runs is shown for the  $N=1K$   $N$ -body model. Middle panels:  $(W_\odot, \alpha, \text{family}) = (1, 2.5, 1)$ . Bottom panels:  $(W_\odot, \alpha, \text{family}) = (7, 2.5, 1)$ .

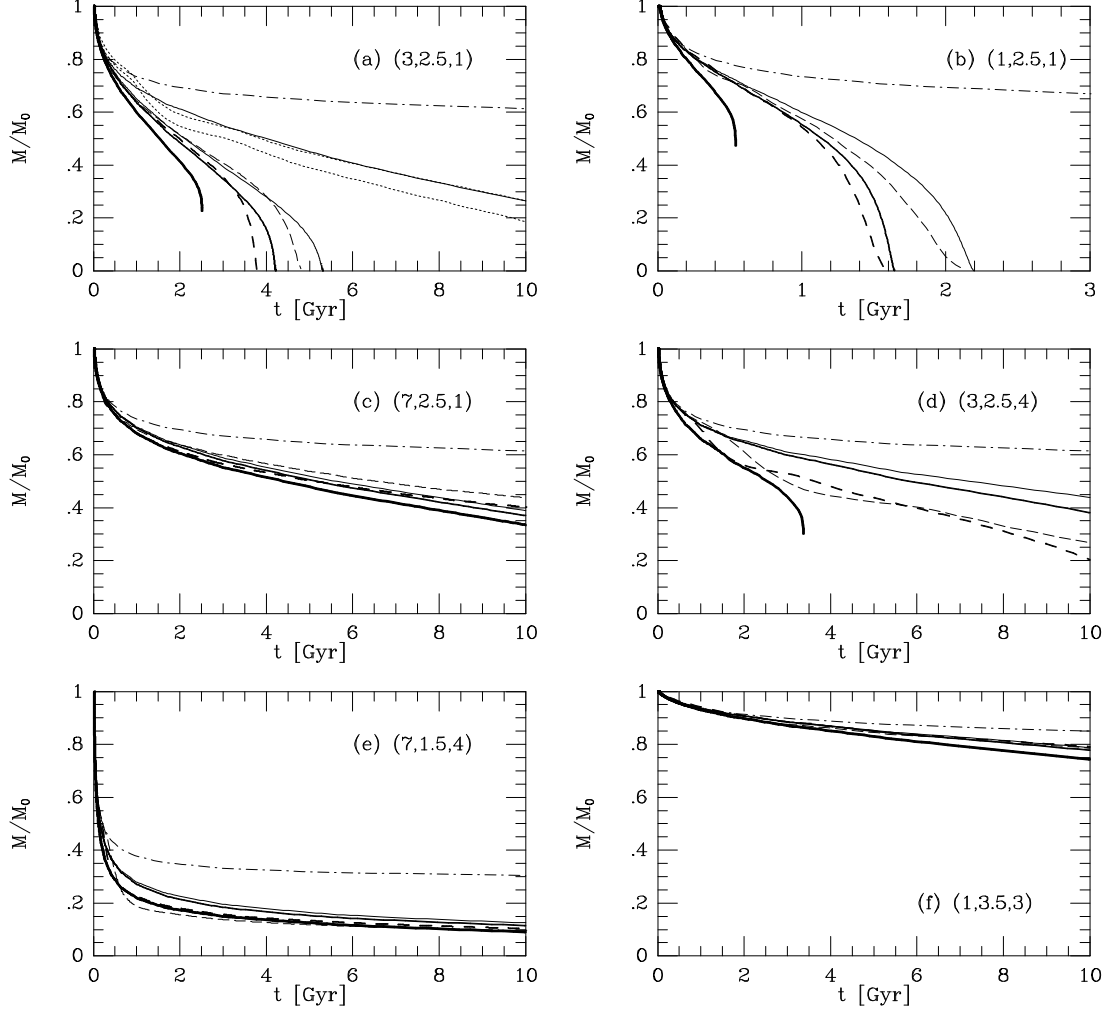


Fig. 2.— Comparison between Aa Fokker-Planck models (solid lines) and  $N$ -body models (dashed lines and dotted lines) for the evolution of the total mass. Thickness of the lines stand for largeness of  $N$ . The thickest solid line in each panel represents the Fokker-Planck model with the instantaneous escape condition, which corresponds to the limit of  $N \rightarrow \infty$ . The other Fokker-Planck models are calculated with the crossing-time escape condition with  $\nu_{\text{esc}} = 2.5$  for finite  $N$ . The dash-dotted lines represent the mass evolution expected when mass loss occurs only through stellar evolution (with no escapers). (a) The initial conditions are  $(W_0, \alpha, \text{family}) = (3, 2.5, 1)$ ;  $N = 1\text{K}, 16\text{K}$ , and  $32\text{K}$ , from right to left. Only for the  $N = 1\text{K}$   $N$ -body model,  $\pm\sigma/2$  deviation from the mean of 10  $N$ -body runs is shown (two dotted-lines). (b)  $(W_0, \alpha, \text{family}) = (1, 2.5, 1)$ ;  $N = 8\text{K}, 16\text{K}$ . (c)  $(W_0, \alpha, \text{family}) = (7, 2.5, 1)$ ;  $N = 4\text{K}, 8\text{K}$ . (d)  $(W_0, \alpha, \text{family}) = (3, 2.5, 4)$ ;  $N = 8\text{K}, 16\text{K}$ . (e)  $(W_0, \alpha, \text{family}) = (7, 1.5, 4)$ ;  $N = 8\text{K}, 16\text{K}$ . (f)  $(W_0, \alpha, \text{family}) = (1, 3.5, 3)$ ;  $N = 8\text{K}, 16\text{K}$ .

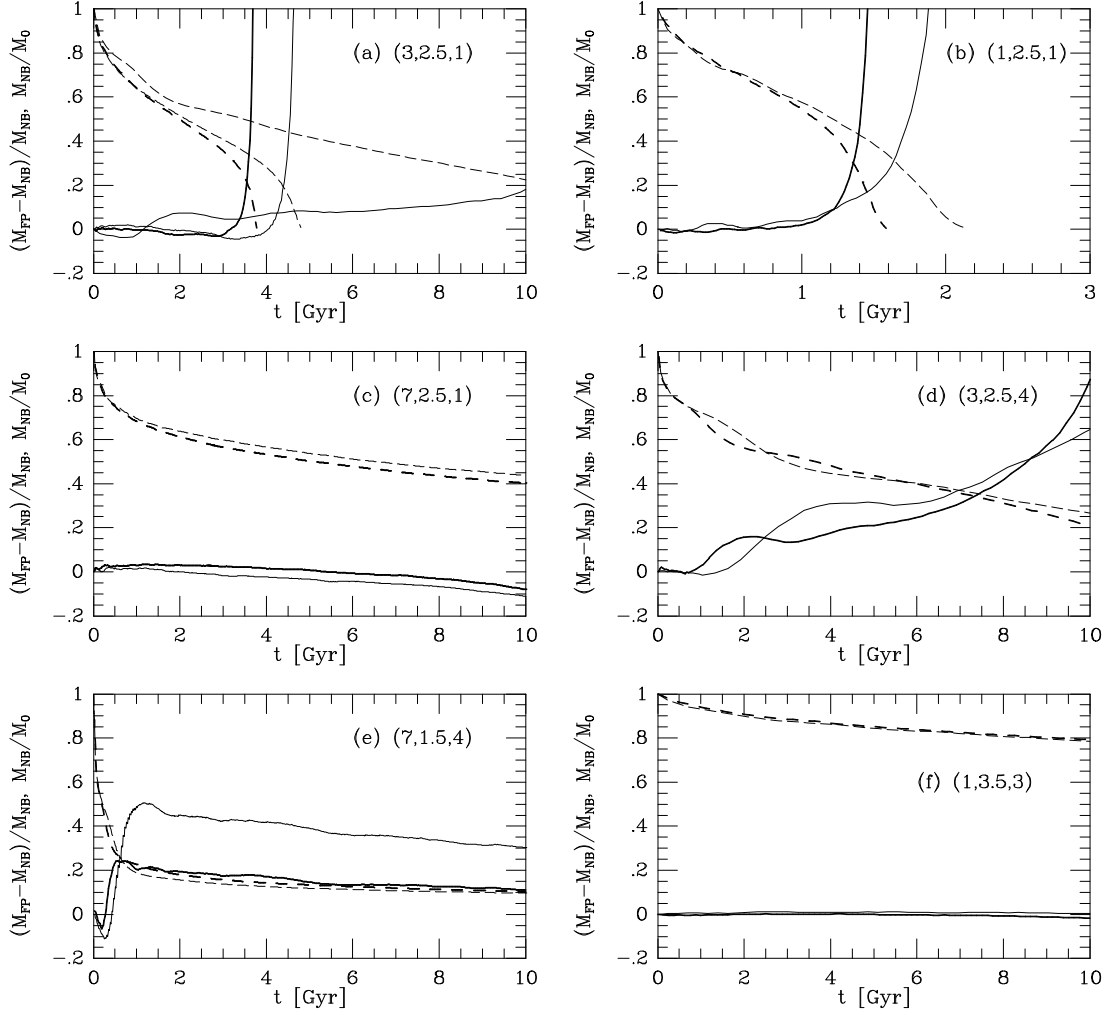


Fig. 3.— Time evolution of the relative mass difference between Fokker-Planck and  $N$ -body models,  $[M_{FP}(t) - M_{N-body}(t)]/M_{N-body}(t)$  (solid lines), for the models shown in Fig. 2. The total mass of the  $N$ -body models is also plotted (dashed lines). In each panel the initial conditions are denoted by three parameters ( $W_0, \alpha$ , family). The thick lines represent the largest- $N$  models in each panel.

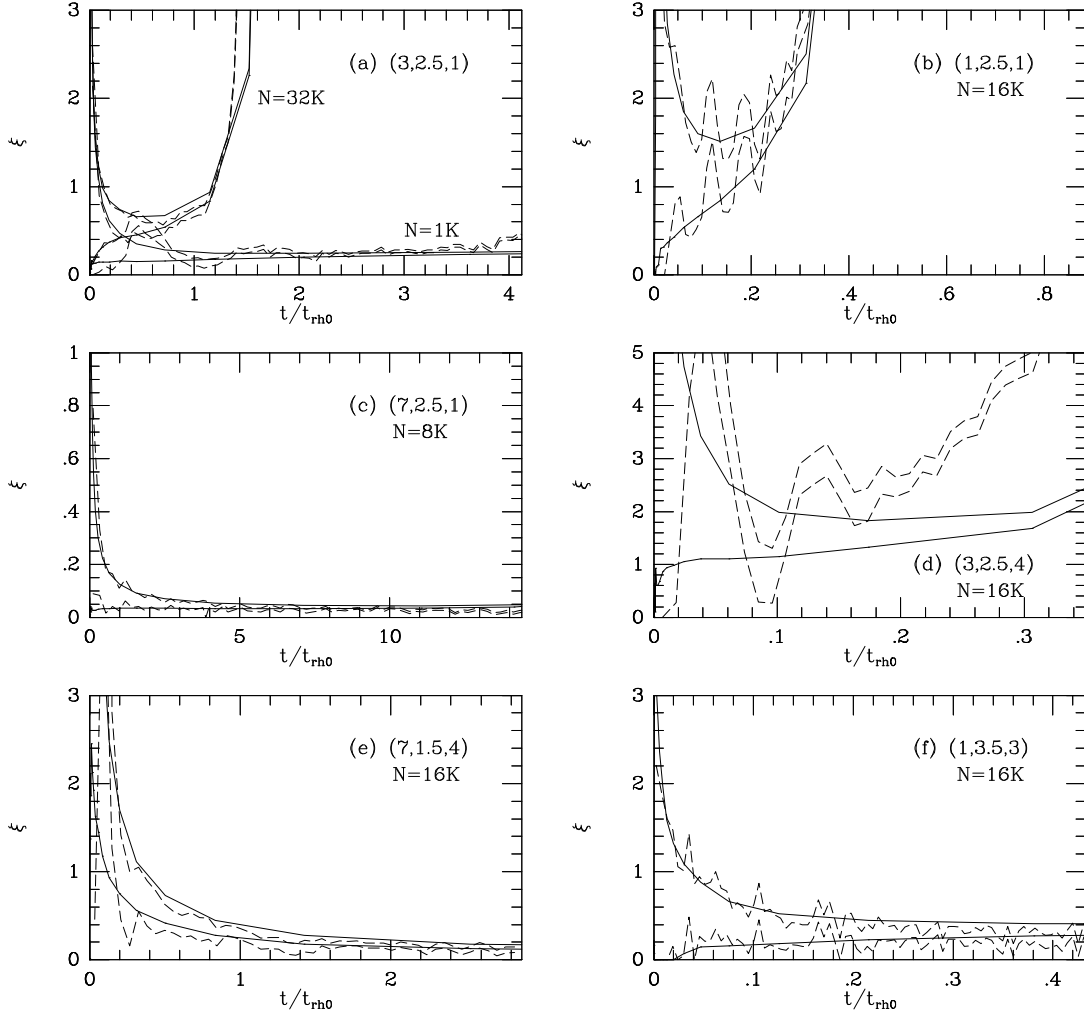


Fig. 4.— Time evolution of the mass loss rates,  $\xi_{\text{tot}}$  and  $\xi_{\text{esc}}$  ( $\xi_{\text{tot}} > \xi_{\text{esc}}$ ), for the Fokker-Planck (solid lines) and  $N$ -body (dashed lines) models shown in Fig. 2. In these plots time is expressed in units of the initial half-mass relaxation time, but for each panel the plotted period is the same as that in Fig. 2 (i.e., 3 Gyr for [b] and 10 Gyr for the others). Only the largest- $N$  models are shown for each set of  $(W_o, \alpha, \text{family})$ , but in (a)  $N=1\text{K}$  models are also shown.

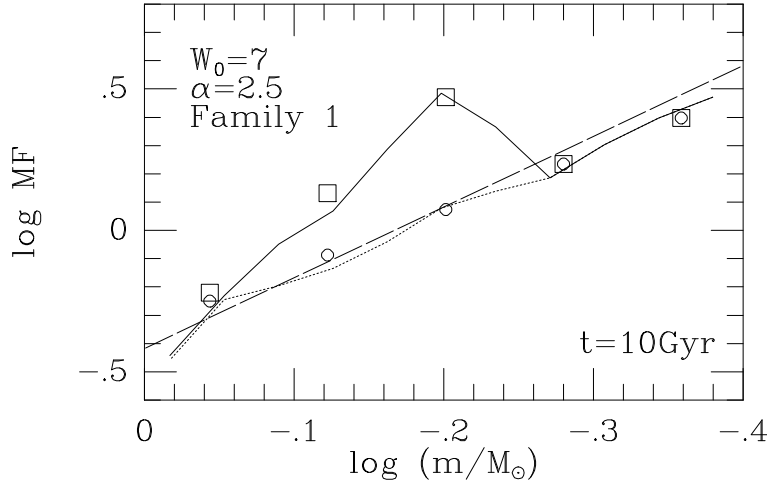


Fig. 5.— The global mass function for the model with the initial conditions of  $W_0 = 7$ ,  $\alpha = 2.5$ , and family 1 at  $t = 10$  Gyr. The dashed line represents the initial mass function. The mass functions are normalized at each epoch. The Fokker-Planck results are given by symbols and the  $N$ -body results are given by lines. The squares and the solid lines represent the mass functions for all the stars, and the circles and the dotted lines represent those for the main-sequence stars only.

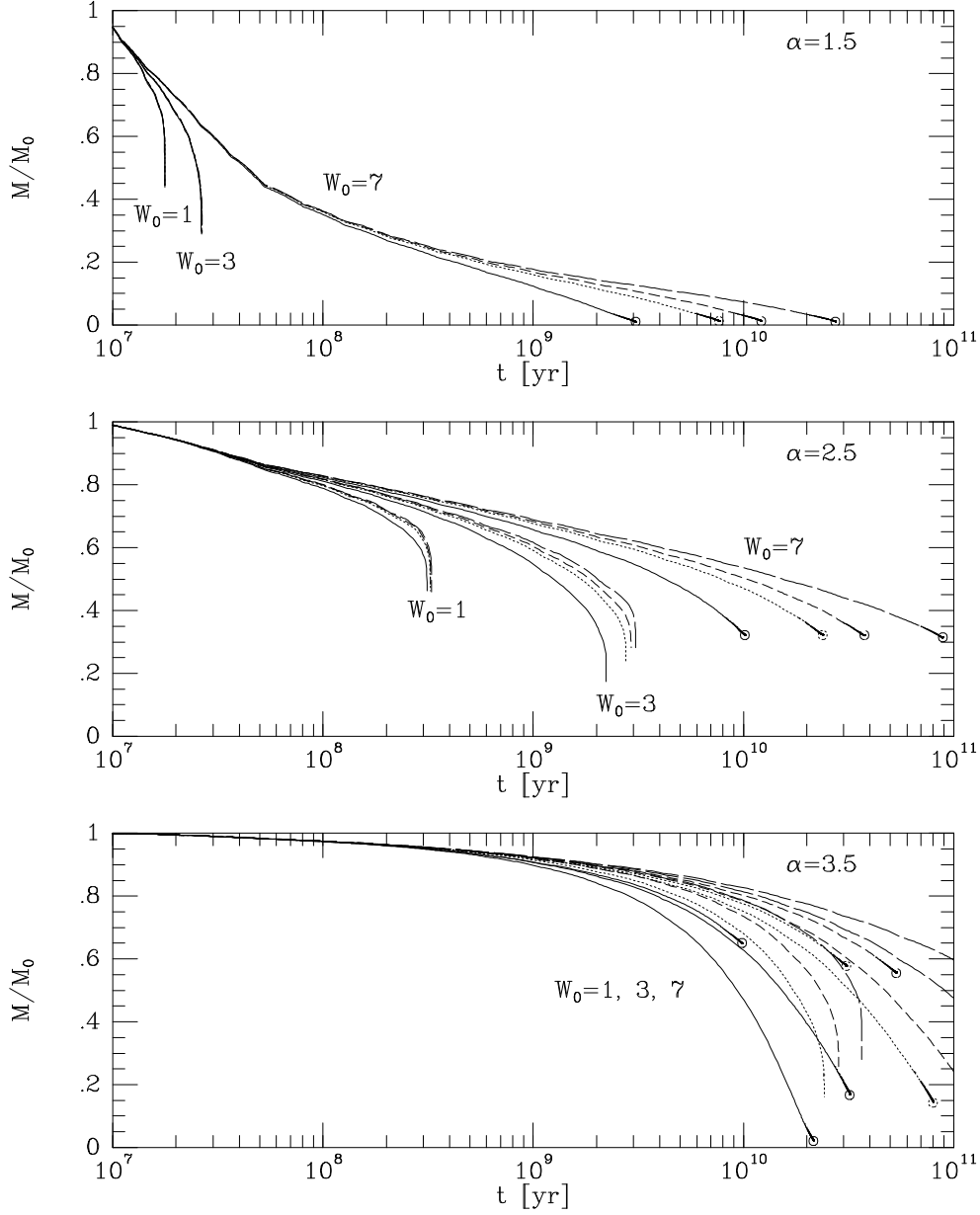


Fig. 6.— Results of the Fokker-Planck survey simulations: Evolution of the total mass. Three panels from top to bottom show results for the initial mass functions of  $\alpha=1.5$ , 2.5, and 3.5. Families 1 to 4 are plotted with solid, dotted, short dashed, and long dashed lines, respectively. The circles at the end points of some lines indicate that those simulations stop at the time of core collapse.



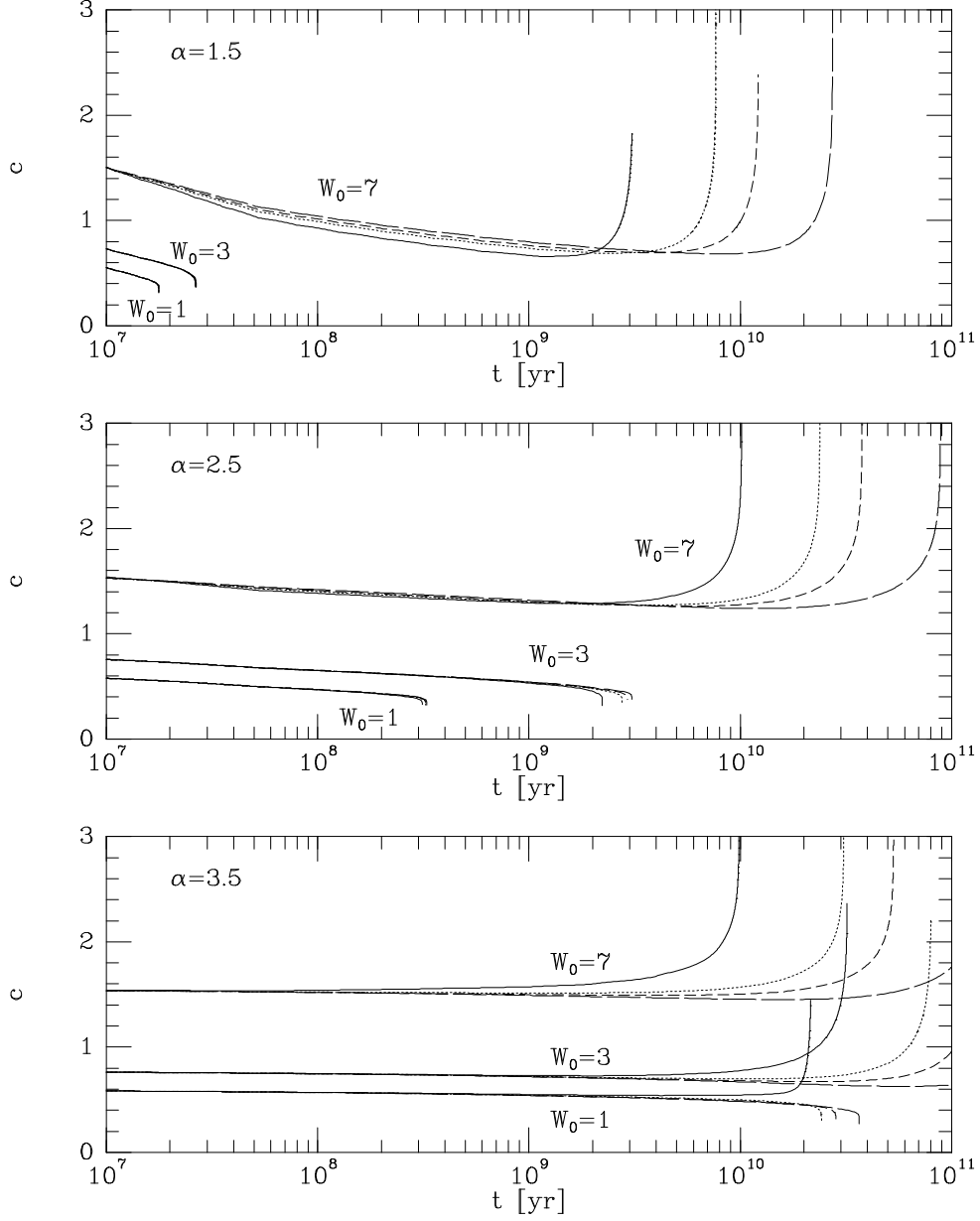


Fig. 7.— Results of the Fokker-Planck survey simulations: Evolution of the concentration  $c$ . The notation in this figure is the same as that in Fig. 6.

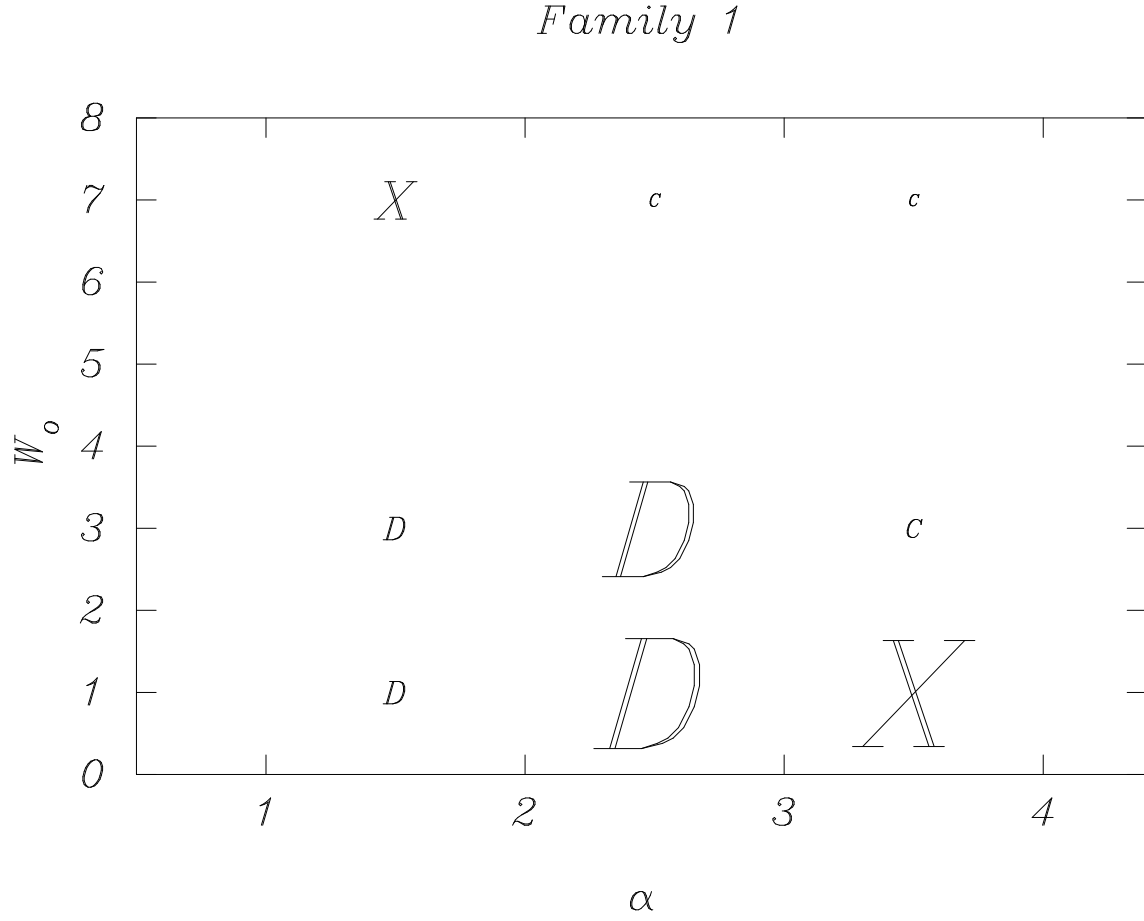


Fig. 8.— Graphical representation of the difference between the Aa models and the CW models in the survey results (see Table 3) for family 1. The power-law index  $\alpha$  of the initial mass function is given along the X-axis and the initial value for  $W_0$  is given along the Y-axis. The symbols  $C$  and  $D$  indicate the end states of the simulations, collapse and disruption, respectively. An  $X$  indicates that the result of CW is disruption where the Aa model reaches core collapse. The size of the letters is proportional to the lifetime at which we arrive as fraction of the lifetime of the cluster calculated by CW; a larger symbol indicates a larger discrepancy.

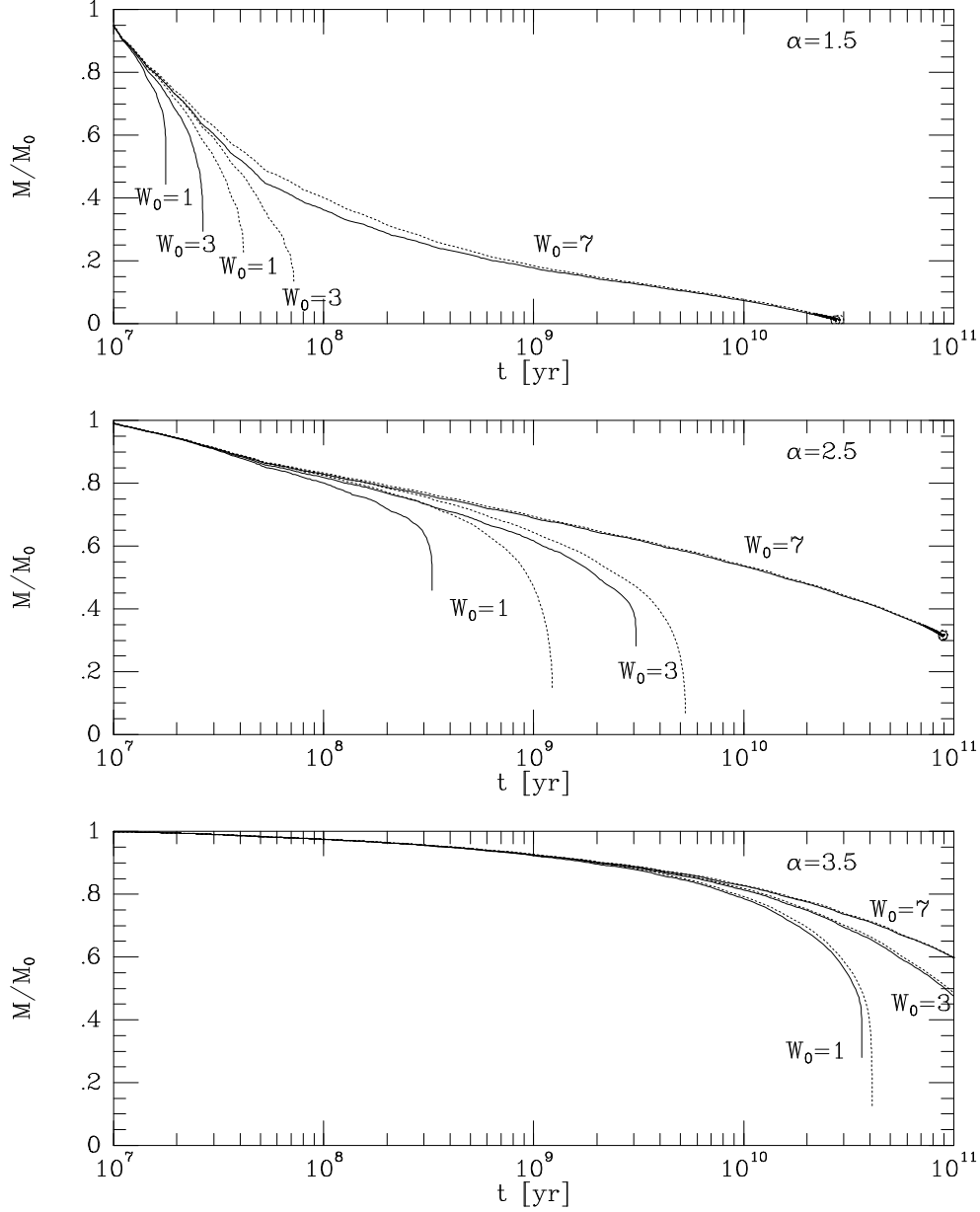


Fig. 9.— Comparison of the mass evolution between the Aa models of  $N = 3 \times 10^5$  clusters (dotted lines) and the Aa models of  $N \rightarrow \infty$  clusters (solid lines, the models shown in Fig. 6). Only the models of family 4 are shown. Three panels from top to bottom show results for the initial mass functions of  $\alpha=1.5$ , 2.5, and 3.5.

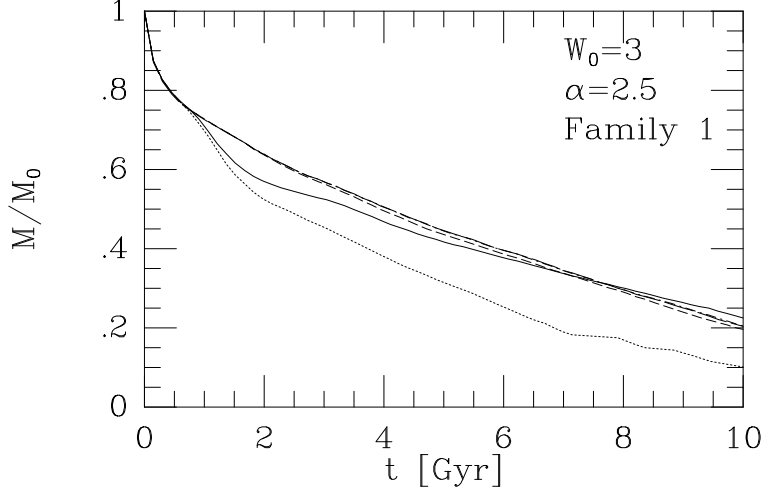


Fig. 10.— Mass as a function of time for various  $N$ -body models with 1K stars (for  $\alpha = 2.5$ ,  $W_o = 3$ , and family 1) for different implementations of the tidal field. Each line represents the mean of ten calculations. The solid line is calculated with a simple tidal cut-off as is used for all other  $N$ -body calculations in this paper. The other lines give the results of calculations with a self-consistent tidal field in which stars are removed beyond the radii  $r_t$  (dotted),  $2r_t$  (short dashed),  $10r_t$  (long dashed), and  $100r_t$  (dash-dotted). The last two lines are almost indistinguishable.

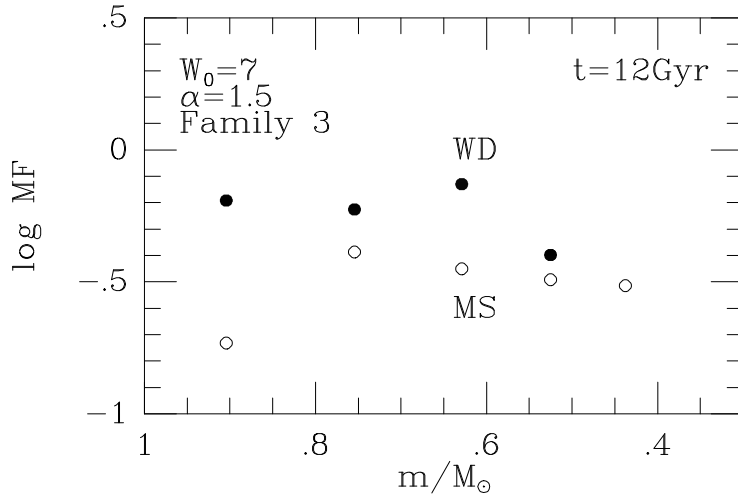


Fig. 11.— The global mass function for the model with the initial conditions of  $W_o = 7$ ,  $\alpha = 1.5$ , and family 3, from the Fokker-Planck survey, at  $t = 12$  Gyr. The open circles represent the mass function of the main-sequence stars, and the filled circles represent that of the white dwarfs.